POLITECNICO
MILANO 1863

SCUOLA DI INGEGNERIA INDUSTRIALE
E DELL'INFORMAZIONE

A Numerical Study on Mechanical Metamaterials in Classical Guitars

Tesi di Laurea Magistrale in
Music and Acoustic Engineering

Author: **Mattia Lercari**

Student ID: 953596
Advisor: Prof. Fabio Antonacci
Co-advisors: Sebastian Gonzalez
Academic Year: 2021-22

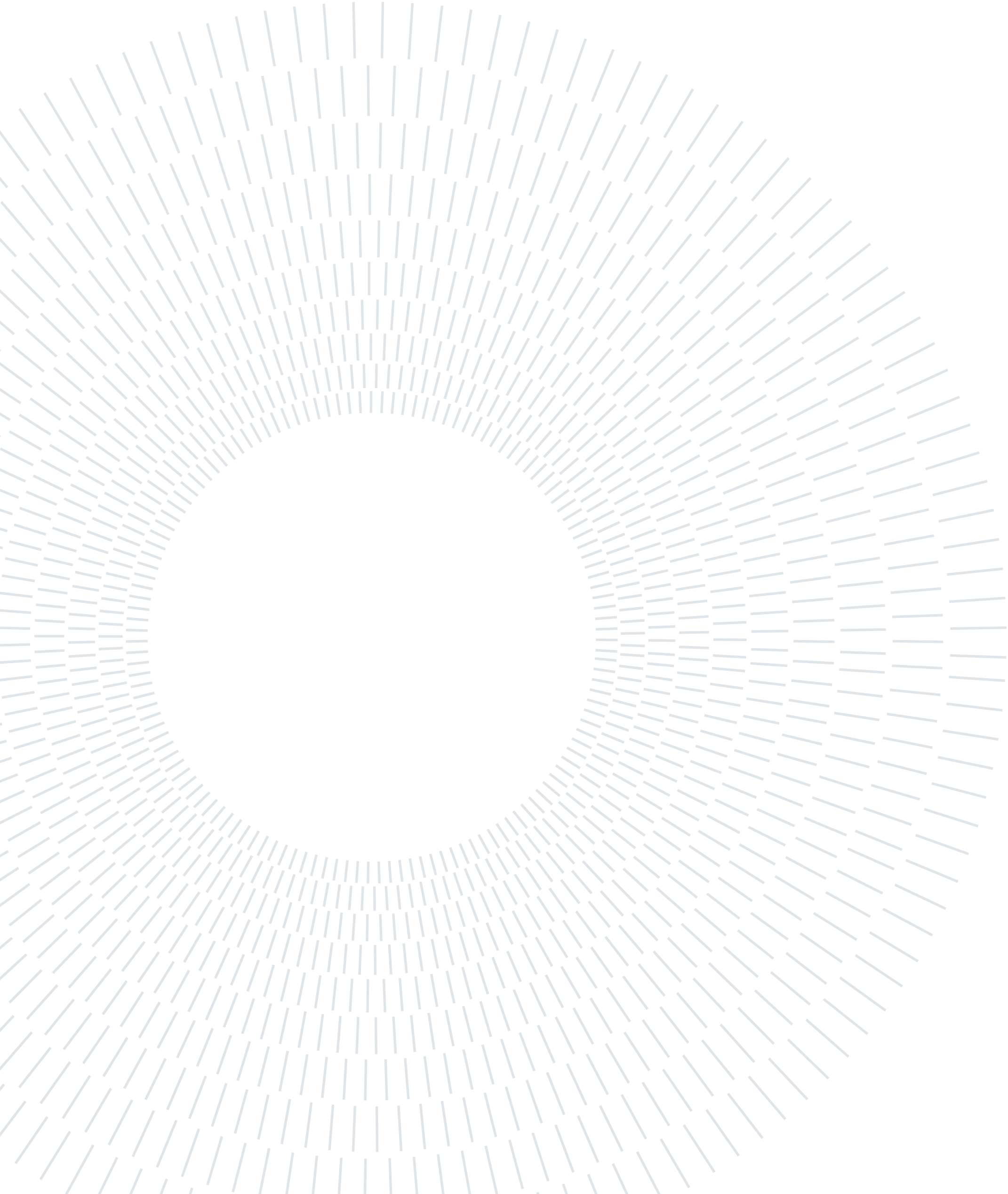

Abstract

Traditionally, wood has been one of the most widely used materials in the construction of musical instruments, as its high stiffness-to-density ratio makes it an excellent sound radiator. Some specific kinds of woods, commonly referred to as *tonewoods*, are held in high regard, as they tend to exhibit just the right mechanical properties necessary to produce high quality instruments. The supplies of these woods, however, are especially prone to shortages due to deforestation or to climate change-related habitat shrinking. Moreover, even within the same species, wood exhibits high variability in its mechanical properties, so only a fraction of the samples from an available supply will be suitable for use in high-end musical instruments. Having the possibility of deliberately engineering the mechanical behaviour of wood would make sourcing the materials easier and cheaper, and it would allow for greater consistency across similar instruments.

Searching for a means to achieve this, we look to the field of mechanical metamaterials for inspiration. Metamaterials are composite materials which exhibit unique mechanical properties derived from their structure rather than their composition and as such, they offer a great deal of control over their properties. The starting point of our work is represented by recent results which show that the mechanical properties of rectangular, thin wooden plates can be purposefully adjusted by carving them with specific patterns of holes, effectively creating a 2D wooden metamaterial. In this thesis we investigate the use of such metamaterials in the soundboards of classical guitars. By way of finite element simulations, we study their effect on the modal behavior and on the mobility frequency response of the instrument, and on its ability to sustain the load exerted by the tension of the strings. Our results show that it is possible, thanks to the metamaterials, to build an instrument which is overall louder than the traditional design without radically altering its timbre, and without compromising its structural integrity. As such, metamaterials have the potential to represent a new and powerful tool in the arsenal of guitar makers.

Keywords: musical acoustics, mechanical metamaterials, classical guitar, finite element modeling

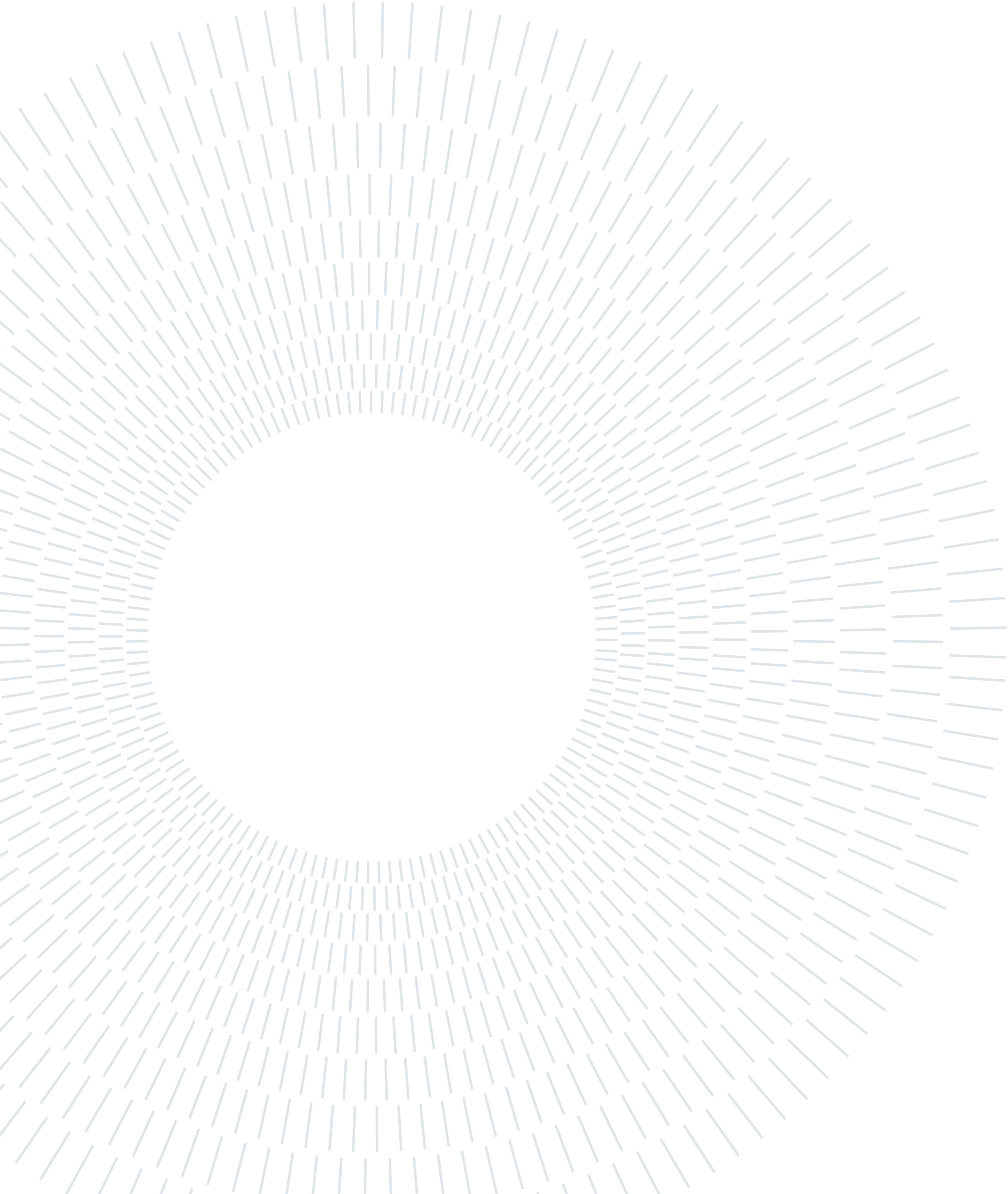

Abstract in lingua italiana

Tradizionalmente, il legno è sempre stato uno dei materiali più usati nella costruzione degli strumenti musicali, essendo un materiale al contempo molto leggero e molto rigido, proprietà che gli permettono di irradiare suono in maniera molto efficiente. Alcuni tipi di legno sono considerati particolarmente adatti all'uso in strumenti musicali di alta qualità, poichè tendono ad esibire le proprietà meccaniche ideali allo scopo. La disponibilità di questi legni, tuttavia, può spesso essere limitata, a causa della deforestazione o del restringimento degli habitat causato dal cambiamento climatico. Il legno, inoltre, presenta proprietà meccaniche estremamente variabili, anche all'interno della stessa tipologia, per cui solo una frazione del legno disponibile ha le caratteristiche adatte per l'uso in strumenti di pregio. Avere la possibilità di intervenire a piacimento sulle proprietà meccaniche del legno, dunque, renderebbe l'approvvigionamento di materiali molto più semplice ed economico.

Con questo scopo in mente, ci rivolgiamo al campo dei metamateriali meccanici in cerca di ispirazione. I metamateriali sono materiali compositi che presentano proprietà meccaniche particolari derivate dalla loro struttura, invece che dalla loro composizione. Il punto di partenza di questa tesi è un recente studio che dimostra che le proprietà meccaniche delle piastre sottili di legno possono essere modificate ad hoc intagliando degli specifici pattern di buchi, creando così un metamateriale 2D su base legnosa. In questa tesi studiamo l'uso di tali metamateriali nelle tavole armoniche delle chitarre classiche. Tramite modellazione a elementi finiti studiamo il loro effetto sui modi di vibrazione e sulla risposta in frequenza dello strumento, nonchè sulla sua capacità di sopportare il carico imposto dalla corde in tensione. I risultati mostrano che è possibile, con questi metamateriali, costruire uno strumento più sonoro senza alterarne radicalmente il timbro caratteristico e senza comprometterne l'integrità strutturale. Ne concludiamo che i metamateriali potrebbero rappresentare uno strumento potente per l'innovazione nella liuteria.

Parole chiave: acustica musicale, metamateriali meccanici, chitarra classica, modellazione a elementi finiti

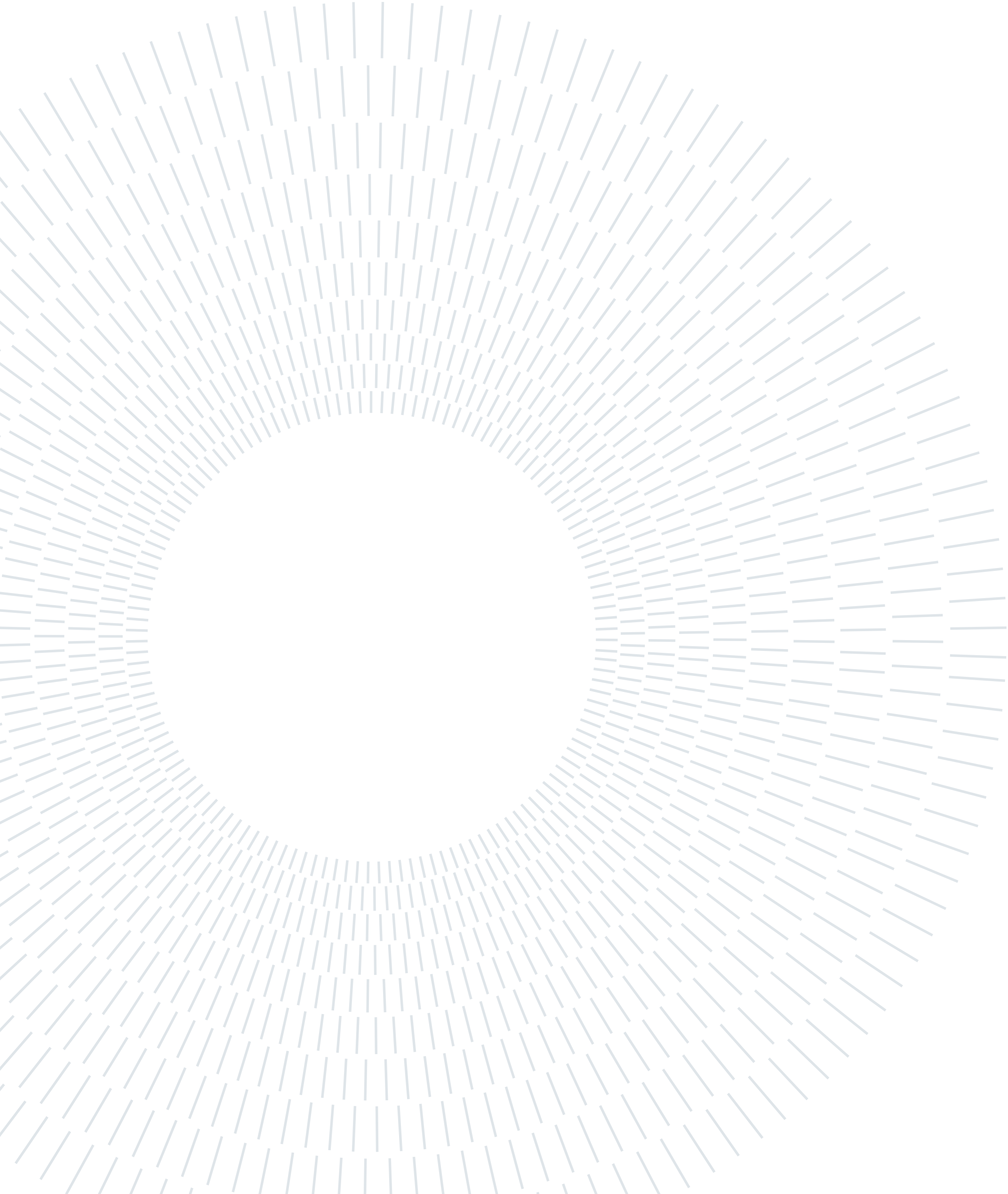

Contents

Abstract **i**

Abstract in lingua italiana **iii**

Contents **v**

Introduction **1**

1 State of the Art and Background **5**

1.1 Mechanics of linear elastic materials 6

1.1.1 The elasticity tensor and the elastic properties of solids 6

1.1.2 Wood as an orthotropic elastic material 7

1.2 Mechanics of thin wooden plates 8

1.2.1 Equation of motion for bending vibration 9

1.2.2 Sound radiation: a merit index 9

1.3 Mechanical metamaterials 11

1.3.1 New materials for musical instruments 12

1.3.2 Wooden metamaterials 14

2 Building a 3D Model of the Guitar **17**

2.1 Construction of the classical guitar's body 18

2.1.1 The outline 18

2.1.2 Soundboard and bracing 18

2.1.3 Back 21

2.1.4 Ribs, tail block and heel block 21

2.1.5 Bridge 22

2.2 Parametric Model of the metamaterial top 22

2.3 Wood choice and mechanical properties 24

3 Finite Element Analysis of the Guitar **27**

3.1 FE Analysis in COMSOL Multiphysics® 28
3.2 Eigenfrequency simulations for modal analysis 28
3.2.1 Modal analysis of the free, unbraced plates 29
3.2.2 Modal analysis of the unbraced plates in simply supported boundary conditions 32
3.2.3 Modal analysis of the free, braced plates 35
3.2.4 Modal analysis of the braced plates in simply supported boundary conditions 39
3.2.5 Modal analysis of the complete body 39
3.3 Deformation under static load 46
3.3.1 Effect of varying hole size and orientation 46
3.3.2 Compensating with the braces 49
3.4 Mobility at the bridge 52

4 Conclusions **57**
4.1 Future Works 59

Bibliography **61**

List of Figures **65**

List of Tables **71**

List of Symbols **73**

Acknowledgements **75**

Introduction

Traditionally, wood has been one of the most widely used materials in the construction of musical instruments. There are, of course many reasons why this is the case. First of all, wood is a relatively abundant and highly workable material and, historically, it would have been readily available to skilled craftspeople who used it to for a plethora of applications. Moreover, the specific mechanical properties of wood in general (and some specific kinds of woods in particular) are greatly beneficial for the construction of an object that must be "loud", i. e. that must radiate sound efficiently. Indeed wood, by its very nature, is a material that exhibits remarkable strength and stiffness (along the grain, at least) despite being generally very light. As we will discuss later, these features are especially desirable in materials for musical instruments [1, 2]. Thus, wood has come to dominate many instrument making traditions, and in particular the tradition of European style stringed instruments, as the undisputed material of choice.

Despite its many advantages, however, this widespread adoption does present some issues. First of all, not all woods are created equal, and some are better than others when it comes to their use in musical instruments (or at least they are traditionally regarded as more desirable). When it comes to the finest instruments, makers are usually quite selective about the species of woods that they use for the various components. Many of these prized species can be in short supply due to deforestation or climate-change related habitat shrinking [3–5]. This issue is compounded by the high variability of the mechanical properties exhibited by single wood species across different samples [6, 7], as not all samples of a given species will exhibit the necessary features. This great variance, together with the increasingly waning supplies, means that sourcing materials with the desired characteristics for the construction of high quality instruments can prove to be a difficult task.

Of course the variability in the properties of the material poses an ulterior problem for makers, that of consistency across different instruments. A luthier could craft many seemingly identical instruments out of the same materials, with the same techniques and dimensions, and the great variance in the mechanical properties of the wood could make it so no two of these instruments would sound the same. While many would argue that this only adds to the charm of each individual piece, on the other hand the lack of consistency prevents the craft from advancing incrementally in a scientific fashion, with the ultimate result of stifling innovation.

With all this in mind, it's clear that having the possibility to deliberately intervene on wood to tune its mechanical response would be greatly beneficial for instrument makers. First of all, it could allow for a more efficient use of the available supply of wood, as samples that would otherwise be discarded could be modified to meet the desired requirements. Instruments could also be manufactured with a wider range of wood species, as woods that aren't usually regarded as appropriate could be adapted suitably, and used in place of other less available types. Greater consistency across different instruments could also be easily achieved, as individual components could be tuned so that the final structure exhibits an established target response. Furthermore, new opportunities for the creation of innovative instrument designs could be opened by a tool or technique capable of giving makers this new degree of control over the materials they use.

In order to find such a tool or technique, we look for inspiration in the field of mechanical metamaterials. Broadly speaking, a metamaterial is a fabricated composite material designed either to mimic known material behavior, or to exhibit a completely novel behavior uncommon in readily available materials [8]. These composites are usually realized by embedding artificial inclusions or inhomogeneities in a host material. The appeal of metamaterials lies in the possibility to directly engineer their properties during fabrication. When it comes to mechanical metamaterials, the last few decades have seen considerable advancements in research and innovation [9]. However, very few studies towards the applications of metamaterials to musical instruments can be found in the literature. One of the few studies that exist, however, has recently shown that the mechanical properties of rectangular, thin wooden plates can be purposefully altered by carving bespoke patterns of circular or elliptical holes, effectively creating a novel tunable wooden metamaterial [10]. These results are promising, and they represent the main inspiration behind the present work. Here we set out to study the effect that using similar metamaterials in the construction of a finished instrument (and in particular the classical guitar) would have on its mechanical behavior, and whether their use would be feasible and beneficial.

Our studies are conducted entirely via finite element analysis. After having realized a 3D model of a classical guitar, inspired by a traditional design, we produced several different variations with elliptical holes carved in the underside of the lower bout of the soundboard, varying the holes' size and orientation. We then proceeded to perform a series of modal studies. First, we studied the eigenfrequencies and the eigenmodes of the soundboards detached from the body, without bracing and in free boundary conditions.

Then, we added simply supported boundary conditions. We repeated both steps for the soundboards with bracings, then, finally, we analyzed the modal behavior of the complete instruments. From the comparison of the effects of the metamaterials in these different cases, we seek to gauge how significant their impact remains when moving from a simple free rectangular plate to a plate with a different shape, with bracings, and mounted to a complex structure. The next part of the work deals with the ability of the instrument to bear the load imposed by the tension of the strings. We performed a series of static simulations aimed at assessing if and how the introduction of the metamaterials affects the stability of the guitar, and how much the soundboard is warped in the different cases. We also investigated how to correct for these adverse effects by adding thickness to some of the braces. Finally, we performed a series of frequency domain simulations of the guitar body, imposing an harmonic load in the bridge area of the soundboard, to recover the frequency response of the instrument. The resulting driving point mobilities were compared to understand the effect of the metamaterials on the sound of the guitar.

This thesis is organized as follows:

- In **Chapter 1** we cover the relevant theoretical background on the theory of elasticity in solids and on the mechanics of thin plates, with a focus on the specific properties of wood and on the mechanical parameters which are most relevant for a stringed instrument's soundboard. We also give a brief review of the literature on mechanical metamaterials, and we present the state of the art on their application to musical instruments.
- In **Chapter 2** we describe how the 3D model of the guitar body was created. We also describe how the hole patterns were created. We then report which wood species were chosen for the various components and how the model of the materials was implemented.
- In **Chapter 3** we give an exhaustive description of the studies that were performed and the results that were obtained. We start from a discussion of the modal analyses that were performed on the soundboard with and without braces and with different boundary conditions and on the complete body of the instrument. We then move on to a series of simulations aimed at assessing the behavior of the instrument under the static load imposed by the tension of the strings. Finally, we report another set of studies that were performed in order to obtain the mobility response spectrum of the instruments. In all cases we compare and discuss the results with different configurations to gain insight into the effect of the metamaterial on the behavior of the instrument.

- Finally, in **Chapter 4**, we elaborate on which conclusions can be drawn from our results and what possible future developments might be needed to build on the present work.

1 | State of the Art and Background

In this chapter we present a summary of the theory of linear elasticity as it pertains to the mechanical characterization of wood. We then present the equation of motion for the bending vibrations of thin plates under the assumptions of Kirchhoff-Love's theory and highlight the relevant elastic constants for an orthotropic plate. In the following section, we introduce the *sound radiation coefficient*, a quantity that has been used in the literature to quantify the efficiency of sound radiation from plates based only on their Young's moduli and densities. We then move on to a brief overview of the literature on mechanical metamaterials, their historical development, and their applications, largely based on a review by Yu et al. [9]. This is followed by a discussion on the use of wood in instrument making, and in acoustical and mechanical metamaterials, before introducing recent results by Gonzalez et al. [10] on wooden metamaterials and their possible applications to the manufacture of musical instruments. These results are of particular relevance here, as they represent the main inspiration behind the present work.

1.1. Mechanics of linear elastic materials

1.1.1. The elasticity tensor and the elastic properties of solids

As far as the stresses and strains involved that are concerned in most structural vibrations, including those at play in stringed musical instruments under normal operating conditions, we can safely assume to be in the elastic domain of the structure's materials. This term [11] refers to the region in the material's stress space where variations in the stresses only lead to variations in the elastic strains, i. e. the strains associated with reversible deformation. Under these conditions, the stress-strain relationship is linear, taking the form of a generalization of Hooke's law to continuum mechanics:

$$\sigma_{ij} = A_{ijkl}\varepsilon_{kl} \tag{1.1}$$

where σ_{ij} is the stress tensor and ε_{kl} is the strain tensor. The fourth-rank tensor A_{ijkl} is the so called *elasticity tensor*, and it completely characterizes the elastic behavior of the material. It has 81 distinct components, but as a consequence of the symmetry of the stress and strain tensors, for an anisotropic elastic material this number is reduced to 21, which allows us to represent it as a symmetric 6×6 matrix.

The simplest situation is that of an isotropic elastic material, i. e. a material whose elastic properties are the same in all directions. In this case, the number of independent components drops down to two: in terms of the *Lamé parameters* λ and μ, (1.1) becomes, using Voigt notation:

$$\begin{pmatrix} \sigma_{xx} \\ \sigma_{yy} \\ \sigma_{zz} \\ \sigma_{zx} \\ \sigma_{yz} \\ \sigma_{xy} \end{pmatrix} = \begin{pmatrix} \lambda + 2\mu & \lambda & \lambda & 0 & 0 & 0 \\ \lambda & \lambda + 2\mu & \lambda & 0 & 0 & 0 \\ \lambda & \lambda & \lambda + 2\mu & 0 & 0 & 0 \\ 0 & 0 & 0 & 2\mu & 0 & 0 \\ 0 & 0 & 0 & 0 & 2\mu & 0 \\ 0 & 0 & 0 & 0 & 0 & 2\mu \end{pmatrix} \begin{pmatrix} \varepsilon_{xx} \\ \varepsilon_{yy} \\ \varepsilon_{zz} \\ \varepsilon_{zx} \\ \varepsilon_{yz} \\ \varepsilon_{xy} \end{pmatrix} \tag{1.2}$$

The elastic tensor in (1.2) can also be defined in terms of two commonly used properties which can be readily measured on samples of the material: the *Young's modulus* E and the Poisson'ratio ν. These, together with the second Lamé parameter μ, which in the context of solid mechanics is more commonly called *shear modulus* and denoted by the letter G, will be the parameters we will use to define the elastic properties of the wood in the numerical model. Let us therefore introduce briefly their definitions and interpretations.

First of all, the Young's modulus is defined as the ratio between stress and strain under uniaxial loading, where only one normal component of the stress and strain tensors is non null:

$$\sigma_{xx} = E\varepsilon_x \tag{1.3}$$

As such, this parameter describes the compressive stiffness of the material. For an isotropic material, the Young's modulus can be written in terms of the Lamé parameters as $E = \frac{\mu(3\lambda+2\mu)}{\lambda+\mu}$.

A sample subject to uniaxial loading, however, doesn't undergo deformation only in the direction of the applied stress, but also in the transverse directions. This is what is referred to as the Poisson's effect, and its extent is described by a dimensionless parameter called *Poisson's ratio*, denoted by the letter ν and defined by the following relations:

$$\varepsilon_{yy} = -\nu\frac{\sigma_x x}{E}, \quad \varepsilon_{zz} = -\nu\frac{\sigma_x x}{E} \tag{1.4}$$

For an isotropic material, the Poisson's ratio can also be written in terms of the Lamé parameters, in the form $\nu = \frac{\lambda}{2(\lambda+\mu)}$. Thus, specifying both E and ν is enough to completely define the elastic tensor in (1.2).

Finally, the shear modulus G is defined by the relation between shear stresses and shear strains; for instance, for the x and y components [12]:

$$\sigma_{xy} = 2G\varepsilon_{xy} \tag{1.5}$$

As already mentioned, in an isotropic elastic material $G = \mu$. It's also useful to report the expression of G in terms of E and ν, which reads $G = \frac{E}{2(1+\nu)}$.

1.1.2. Wood as an orthotropic elastic material

While many materials can be modelled effectively as isotropic with regards to their mechanical properties, wood is not one of them. However, even in anisotropic materials some symmetries can be found which reduce the number of independent parameters needed to fully specify their elastic properties. This applies to wood as well, which can be considered to be *orthotropic*.

A medium is said to be orthotropic with respect to a given property if said property is invariant under rotation on two orthogonal planes (which implies rotational symmetry on the third orthogonal plane as well). The axes of symmetry for these planes are the principal axes of the material. This kind of symmetry makes it so that the elasticity tensor only has 9 independent components. Equation (1.1) takes the form:

$$\begin{pmatrix} \varepsilon_{xx} \\ \varepsilon_{yy} \\ \varepsilon_{zz} \\ \varepsilon_{zx} \\ \varepsilon_{yz} \\ \varepsilon_{xy} \end{pmatrix} = \begin{pmatrix} \frac{1}{E_L} & -\frac{v_{RL}}{E_R} & -\frac{v_{TL}}{E_T} & 0 & 0 & 0 \\ -\frac{v_{LR}}{E_L} & \frac{1}{E_R} & -\frac{v_{TR}}{E_T} & 0 & 0 & 0 \\ -\frac{v_{LT}}{E_L} & -\frac{v_{RT}}{E_R} & \frac{1}{E_T} & 0 & 0 & 0 \\ 0 & 0 & 0 & \frac{1}{2G_{LT}} & 0 & 0 \\ 0 & 0 & 0 & 0 & \frac{1}{2G_{TR}} & 0 \\ 0 & 0 & 0 & 0 & 0 & \frac{1}{2G_{RL}} \end{pmatrix} \begin{pmatrix} \sigma_{xx} \\ \sigma_{yy} \\ \sigma_{zz} \\ \sigma_{zx} \\ \sigma_{yz} \\ \sigma_{xy} \end{pmatrix} \tag{1.6}$$

where the subscripts L, R and T refer to the principal axes of wood, which are identified by the directions of the fibers and of the growth rings, as shown in Fig. 1.1. The 12 constants appearing in (1.6) (three Young's moduli, three shear moduli, and six Poisson's ratios) are not independent of each other; the Young's moduli and Poisson ratios are related by the following equations:

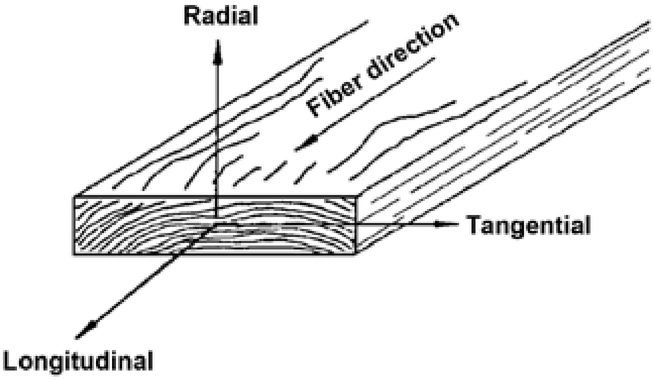

Figure 1.1: The three principal axes of wood, from [13]. The picture shows the direction of the fibers, which coincides with the longitudinal axis, and the growth rings, which are perpendicular to the radial axis.

$$\frac{\nu_{ij}}{E_i} = \frac{\nu_{ji}}{E_j}, \qquad i \neq j, \ i,j = L,R,T \tag{1.7}$$

To fully characterize the elastic behavior of wood, therefore, it is sufficient to specify the shear and Young's moduli and three of the Poisson's ratios.

1.2. Mechanics of thin wooden plates

1.2.1. Equation of motion for bending vibration

The preceding discussion regards the elastic deformation of the bulk material in all three spatial dimensions. However, an object where one of the dimensions is significantly shorter than the others (such as a guitar soundboard) can be accurately described as a 2D system. The most common model used for the description of bending vibrations in such systems is Kirchhoff-Love's theory of thin plates. Under these assumptions, the equation of motion for an homogeneous and isotropic plate is written as [14]:

$$\rho h \frac{\partial^2 w}{\partial t^2} + D\nabla^4 w = 0 \tag{1.8}$$

where w is the out-of-plane component of the displacement, ρ is the material's density, h is the plate thickness, and the symbol ∇^4 denotes the square of the Laplacian operator. The constant D, sometimes referred to as the plate's bending stiffness, is defined as $D = \frac{Eh^3}{12(1-\nu^2)}$.

For an orthotropic plate, the elastic properties differ in the x and y directions. As such, (1.8) becomes:

$$\rho h \frac{\partial^2 w}{\partial t^2} + D_1 \frac{\partial^4 w}{\partial x^4} + D_3 \frac{\partial^4 w}{\partial y^4} + (D_2 + D_4) \frac{\partial^4 w}{\partial x^2 \partial y^2} = 0 \tag{1.9}$$

where the stiffness constants are defined as:

$$\begin{aligned} D_1 &= \frac{E_x h^3}{12\,(1-\nu_{xy}\nu_{yx})}, \quad D_2 = \frac{E_x \nu_{yx} h^3}{6\,(1-\nu_{xy}\nu_{yx})} = \frac{E_y \nu_{xy} h^3}{6\,(1-\nu_{xy}\nu_{yx})}, \\ D_3 &= \frac{E_y h^3}{12\,(1-\nu_{xy}\nu_{yx})}, \quad D_4 = \frac{G_{xy} h^3}{3} \end{aligned} \tag{1.10}$$

The bending vibrational properties of orthotropic thin plates is therefore governed by four elastic constants: the Young's moduli along the two in-plane principal directions, the in-plane shear modulus, and either one of the two Poisson ratios ν_{xy} and ν_{yx}. Guitar soundboards are usually made of quarter-sawn wood, where the in-plane principal directions correspond to the longitudinal and radial axes, as shown in Fig. 1.2.

1.2.2. Sound radiation: a merit index

Having estabilished a model for the study of thin plates, we now ask ourselves how the properties of the material influence the sound generated by such a structure. In the literature on the topic [1, 2] we can find a proposed merit index for the efficiency of the sound radiation, which only depends on the Young's moduli and density of the plate's

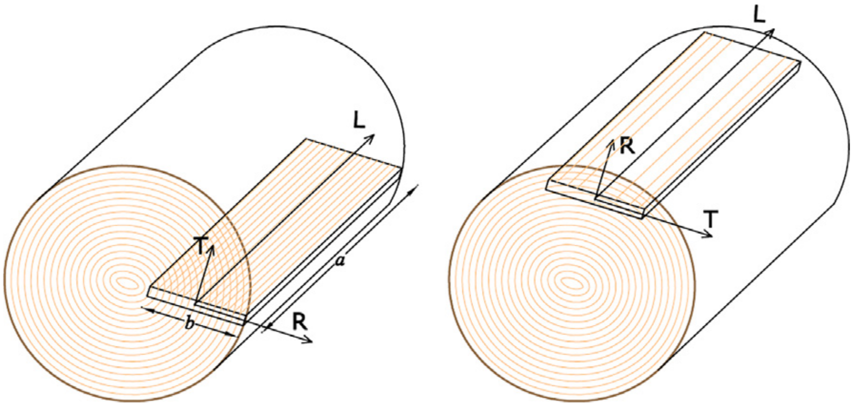

Figure 1.2: Comparison of a *quarter sawn* (left) and a *plain sawn* board, showing the reference frame of the principal axes of the wooden log. Image from [15].

material. This is a good target metric for acoustic instruments, as a poor efficiency of transduction between the mechanical and acoustic domain cannot be compensated by electrical sound reinforcement. In the following we present an argument for the definition of the index taken from [1].

The loudness of the sound radiated from a plate-like structure (such as a soundboard) is directly related to the magnitude of its mechanical admittance (also referred to as mobility), which is defined in the frequency domain as:

$$\mathbf{Y}(\omega) = \frac{\mathbf{v}(\omega)}{\mathbf{F}(\omega)} \tag{1.11}$$

where $\mathbf{v}(\omega)$ and $\mathbf{F}(\omega)$ are the velocity on the plate's surface and the applied force, respectively. In general these are taken at any point on the plate, but we will restrict our discussion to the driving-point admittance, i. e. the admittance obtained by taking the velocity at the point where the force is applied. This point in stringed musical instruments will correspond with the location of the bridge, as we will discuss in Chapter 3.

From [16] we know that the mean value of the driving-point admittance for a finite plate coincides with the driving point admittance for an infinite plate. For an isotropic plate this is:

$$Y = \frac{1}{4h^2}\sqrt{\frac{3(1-\nu)}{E\rho}} \tag{1.12}$$

We seek to alter the parameters in (1.12) in order to increase the value of Y. However, we cannot do so indiscriminately: an instrument's soundboard is carefully tuned to have a specific “signature" frequency response, and this is a feature that we want to preserve if we want to produce an instrument that sounds as expected. The tuning is primarily done by adjusting the thickness of the plate. As a measure of the tuning we will take the modal density, which for an isotropic plate this can be written as:

$$n(\omega) = \frac{A}{2\pi h}\sqrt{\frac{3(1-\nu)}{E}} \tag{1.13}$$

where A is the area of the plate. Having fixed the modal density, (1.13) defines the required thickness h. We can then substitute h in (1.12), finding that $Y \propto \sqrt{E/\rho^3}$. We can thus define the *sound radiation coefficient* as[1]:

$$R = \sqrt{\frac{E}{\rho^3}} \tag{1.14}$$

Raising this quantity will increase the mean value of the admittance, resulting in a "louder" plate. The definition of this index underscores the necessity for materials that are both very stiff and very light. As one would expect, woods typically used in the manufacture of soundboards tend to have remarkably high values of R. However, the last few decades of developments in materials engineering have opened the possibility of deliberately controlling these parameters, as we will see in the next section.

1.3. Mechanical metamaterials

A metamaterial is a fabricated composite material designed either to mimic known material behavior, or to exhibit a new behavior that isn't commonly observed in readily available materials [8]. These composites are often realized by way of artificially fabricated inclusions or inhomogeneities embedded in a host medium or connected to or embedded on a host surface. Their appeal lies in the potential to deliberately engineer their physical properties for a wide variety of applications.

The concept of metamaterial first appeared in optics [17, 18], but it was soon applied to acoustics and mechanics [19, 20]. Our interest in the present work is mainly in the applications of these concepts to mechanics. Mechanical metamaterials differ from regular composites in that, ultimately, their mechanical properties depend on the geometries of their subunits rather than from their material composition [9]. In the past decades, a wide variety of such materials has been developed, exhibiting a wide array of enhanced mechanical properties: materials with zero or negative Poisson ratio [21, 22], vanishing

---

[1] For an orthotropic material the definition is

$$R = \frac{[E_x E_y]^{1/4}}{\rho^{3/2}}$$

shear modulus [23], negative stiffness [24], negative compressibility [25] and many other properties that aren't observed in conventional materials.

The manufacturing of musical instruments is far from the only context in which materials that are simultaneously very stiff and very light can be useful. Indeed, many different classes of metamaterials exhibiting remarkable stiffness-to-density ratios have been developed [26], varying widely both in their construction and in their mechanical behavior. Examples include micro/nanolattices, chiral metamaterials, origami-like metamaterials and hierarchical metamaterials [9].

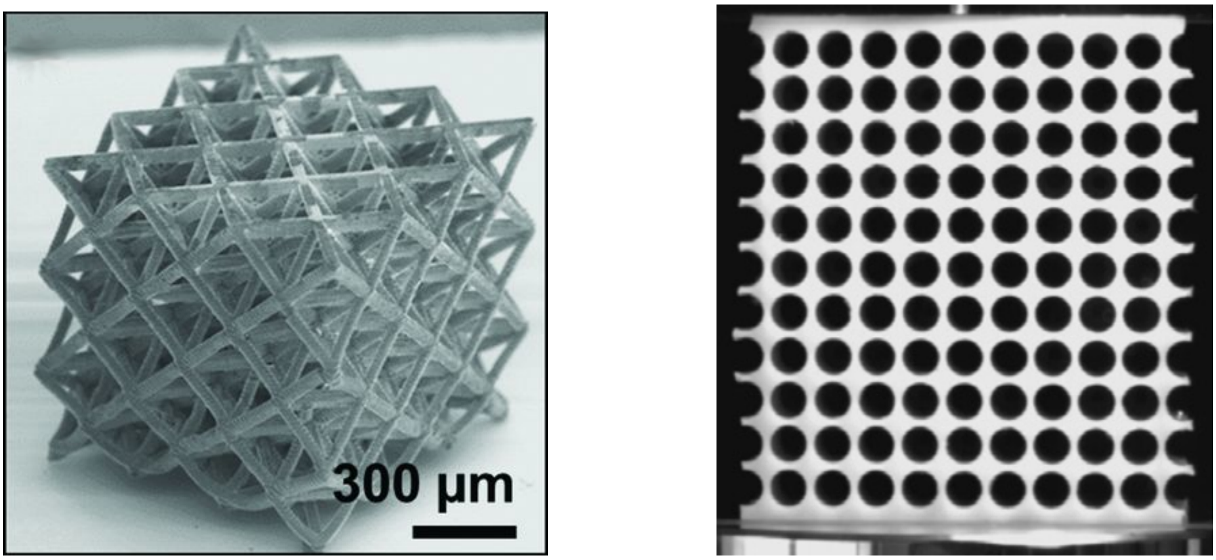

Figure 1.3: (a) Octet-truss unit cells packed into a cubic microlattice [26]. This material exhibits vary high stiffness-to-density ratio. (b) 2D periodic porous structure, from [21]. The mechanical properties of this structure can be controlled by compressing it.

When it comes to the use of metamaterials in the construction of musical instruments, research is very scarce. To the best of our knowledge, only two works exist. One is a work by Bader et al. [27], where the authors apply a ring of masses to the membrane of a frame drum, leading to a cloaking behavior. The other one is a work by Oñate et al., that shows that the application of a sample of a tunable mechanical metamaterial to the soundboard of a guitar can modify the acoustic power spectrum of the instrument.

1.3.1. New materials for musical instruments

Wood has traditionally been the material of choice for musical instruments, and for good reason: we have already discussed how it is particularly well fit for structures that need to radiate sound efficiently. However, the use of wood in this context doesn't come without problems.

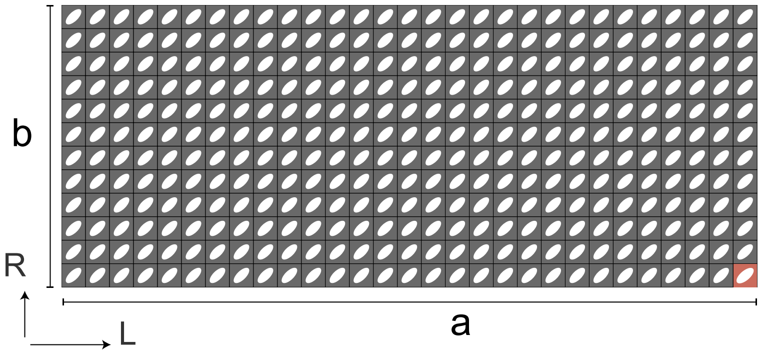

Figure 1.4: Example diagram of a wooden plate carved with a pattern of elliptical holes, from [10]. The image shows a periodic pattern obtained by the repeated juxtaposition of a unit cell. The authors varied the holes' size, aspect ratio and orientation to investigate the effect of these changes in the geometry on the elastic behavior of the plates.

First of all, not all woods are equally apt for use in musical instruments, with regards to their physical properties. Even fewer are those that are widely adopted, for a mixture of technical reasons, aesthetic considerations, and desire to adhere to tradition. The supply of these varieties of woods (commonly referred to as *tonewoods*) is prone to shortages due to deforestation [3] or to climate change-related habitat shrinking [4, 5]. Thus, sustainable sourcing of tonewoods is already an issue for makers, and it could become harder in the coming decades. All of this is compounded by a second problem, that of the high variability of physical properties between different samples of the same wood [6]. This further restricts the availability of high quality tonewood. Moreover, even within selected woods for musical instruments, the variation in density and mechanical constants can be as high as 20% [7], which represents an inconvenience for manufacturers who could benefit from a material that performs reliably across different samples.

In light of these issues, it's clear how finding suitable substitute materials could be of great use for guitar makers. Many have been using carbon fiber in their instruments [28, 29]. Composite materials have also been used commercially, as in the case of Ekoa®, developed by Blackbird Guitars [30]. In the academic literature we can find at least one work proposing the use of a composite with adjustable mechanical properties [31]. However, our interest throughout this work isn't to find a strictly new material for the manufacture of musical instruments, but rather to investigate how we can modify thin wooden plates in order to control and enhance their vibroacoustic properties. This approach has the advantage of meeting the current aesthetic and tonal preferences of luthiers and players, while still offering the possibility to make better use of the existing supply of wood by artificially improving the grading of samples that don't meet requirements. Such improvements could be achieved by using wood as a substrate for the development of mechanical metamaterials.

1.3.2. Wooden metamaterials

Most of the examples discussed in our brief review on metamaterials are constructed out of polymers and man-made materials. Nevertheless, examples of the use of wood as a substrate for metamaterials can be found in the literature, both in structural [32] and acoustical [33] applications. The present work is predominantly inspired by the findings in [10], where the authors show, first by way of simulations and then with experiments, that the effective elastic parameters of rectangular thin wooden plates can be selectively adjusted by carving patterns of holes such as those shown in Fig. 1.4. The authors studied various geometries of such hole patterns, all with elliptical holes in a lattice with a square unit cell with a 20 mm long side. The holes' sizes, aspect ratios, and orientation were varied independently throughout the study to investigate how changing them would affect the mechanical properties of the plates. The ultimate aim here is to understand whether it's possible to use these geometrical parameters to tune the mechanical response of a wooden plate. Both the simulations and the experimental results suggest that this is indeed the case. In particular, it seems that it's possible to obtain a strong reduction in density accompanied by a comparatively low decrease in stiffness, in particular for the case of elliptical holes oriented with their major axis parallel to the longitudinal axis of the wood (see Fig. 1.5). This, as already discussed, is desirable in soundboards for stringed instruments, and it results in an increase of the sound radiation coefficient R for increasing hole size.

As promising as the results are, they have been obtained for the case of rectangular plates in free boundary conditions. Musical instrument soundboards are less straightforward systems: they usually have more complex shapes, they are mounted to and interact with the instrument's main body, and they they're almost always reinforced with braces, as is the case for the piano and the guitar. These factors lead us to question whether the expected improvements introduced by the use of metamaterials would translate clearly to a finished instrument. Therefore, studies about metamaterial structures in complete musical instruments are needed to evaluate if such designs are feasible and/or beneficial. At the time of writing, the only such study is Marelli's master thesis [34], which is about the use of wooden metamaterials like the ones we described in the *tapa* of a *cajón peruano*. The *tapa* is a rectangular plywood board, without braces, so it's very similar to the rectangular plates we have just seen. The metamaterial *tapas* exhibit the expected mechanical behavior on their own, but the results are less clear-cut for the simulations of the complete instrument coupled with the acoustic field. The differences in the frequency response with respect to the regular instrument are hardly appreciable, and the most noticeable changes are in the modal shapes at high frequencies.

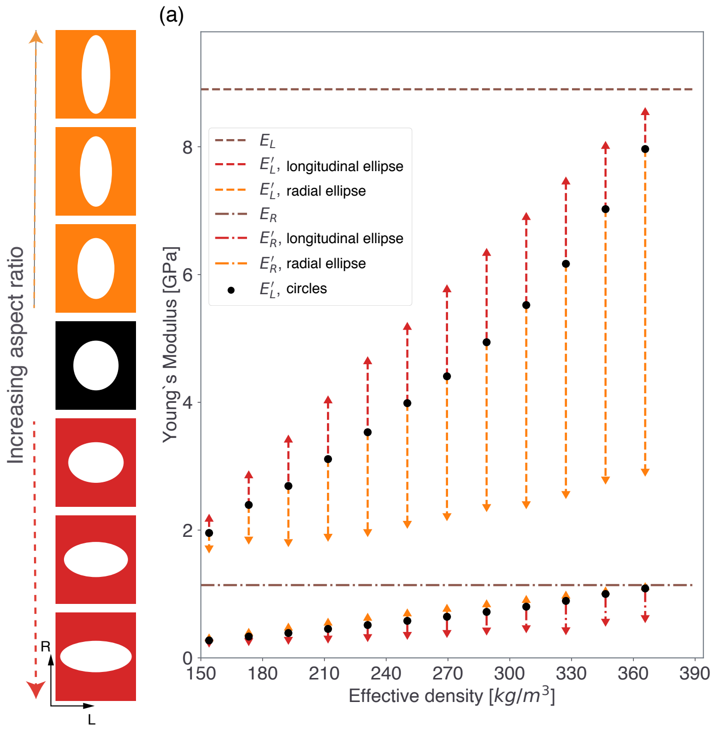

Figure 1.5: Variation of the longitudinal and radial Young's moduli of the plates when varying the aspect ratio of the holes, for different effective densities, from [10]. The terms “longitudinal" and “radial", here as well as in later chapters, refer to the orientations of the holes' major axes with respect to the principal axes of the wood, as shown in the diagram reported alongside the graph. For the longitudinal modulus, the introduction of the holes results in a lowering of the value. The effect is compensated when the major axis of the ellipses is parallel to the longitudinal axis of the plate's wood, and it is accentuated when it's parallel to the radial axis. For the radial modulus, we see an analogous effect.

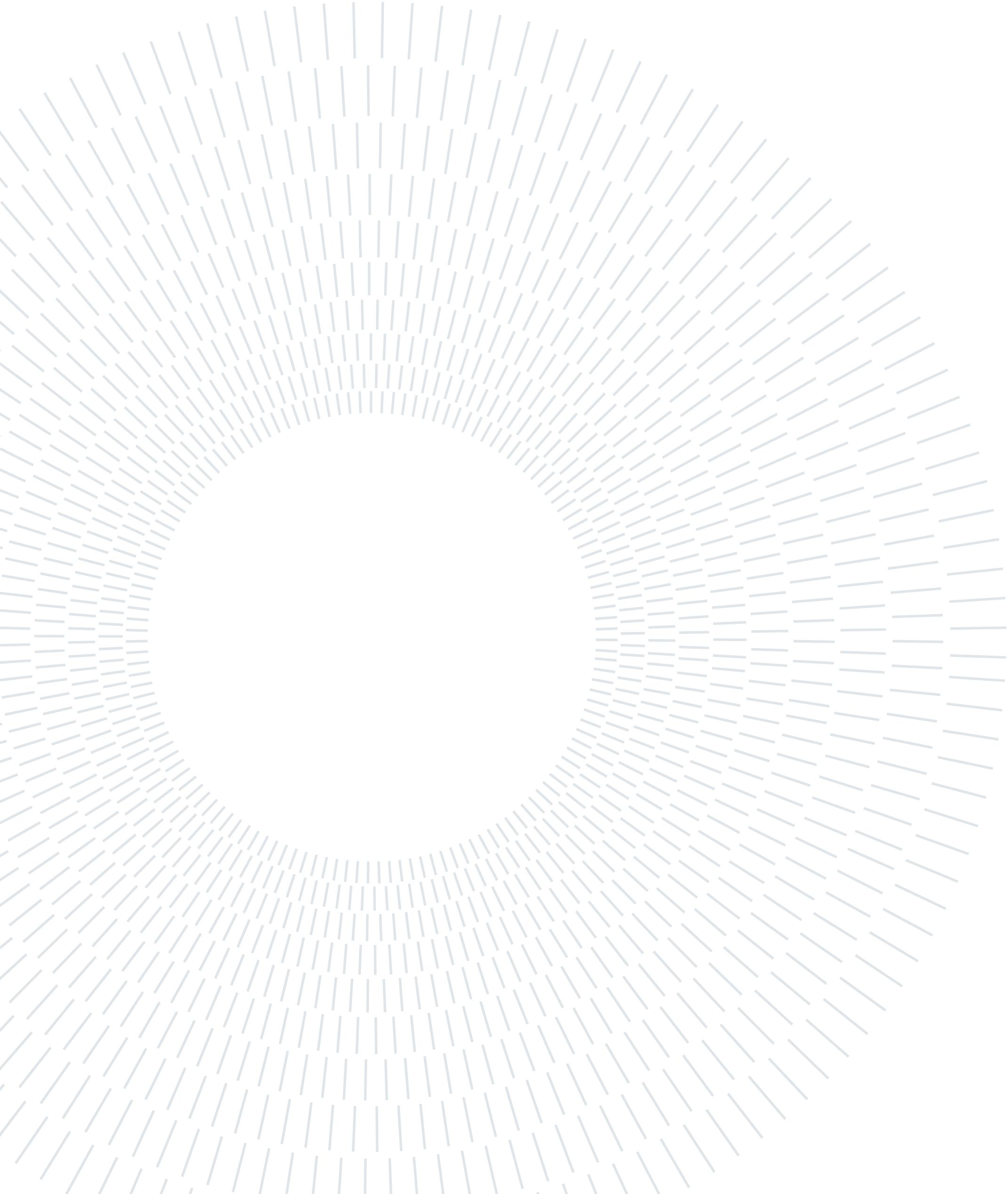

2 | Building a 3D Model of the Guitar

This chapter describes the process of creating a 3D reference model of the guitar body. This was done using Autodesk Fusion 360®, a commercial CAD + CAM software.

Much of this model, and in particular the strutting of the soundboard, follows a traditional design by Antonio de Torres, as described in [35]. Torres, whose work spans the second half of the 19-th century, is widely credited with perfecting and popularizing the so-called "fan"-strutting design, which has since become a staple of classical guitar construction. An exhaustive account of Torres's life and works has been given by luthier José Romanillos in [36] .

A detailed description of how the hole patterns that make up the metamaterial were realized is also given, as well as a description of the choice of the woods for the various components and the related elastic constants.

2.1. Construction of the classical guitar's body

The guitar, as most musical instruments, is a sophisticated piece of fine craftsmanship, constructed by careful assembly of many individual components (see Fig. 2.1). To build a numerical model, some degree of simplification is going to be needed, and this applies to our case too: accordingly, we modeled, first of all, only the main part of the body, omitting the neck and the strings, as we are primarily interested in the efficiency of the mechanoacoustical transduction from the body and soundboard. We are also included a model of the bridge, but it has only been used in stationary simulations, as will be explained in Chapter 3.
Further adaptations have been made both for ease of modeling and as a way to reduce the amount of fine geometrical detail of the model, which results in added computational cost in the FE simulations. For instance, the linings at the joints between the ribs and the back/top plate have been ignored. Moreover, while guitar makers will usually vary the thickness of the soundboard and of the back plate throughout their extent, constant thicknesses were used here in both plates. Finally, whereas most handcrafted instruments will exhibit a curvature both in the top and in the back plate, the former has been modeled completely flat. The curvature of the back plate, however, has been included, since it is usually more pronounced.

2.1.1. The outline

The outline was obtained by tracing the drawing in Fig. 2.2 and interpolating with spline curves. This design, as reported in the drawing, has a length of 483 mm, while the width is 272 mm at the upper bout, 235 mm at the waist, and 360 mm at the lower bout.

2.1.2. Soundboard and bracing

The soundboard was obtained via extrusion from the outline. It is 2.5 mm thick and it has a circular soundhole with a radius of 42.5 mm.

The bracing has also been designed following closely the drawing in Fig. 2.2.The "fan"-struts, "V"-struts and the three struts in the upper bout have been left flat on top, whereas many makers would work them to have a curved or triangular section. The harmonic bars have a rectangular section as well, and they have been scalloped towards the ends.

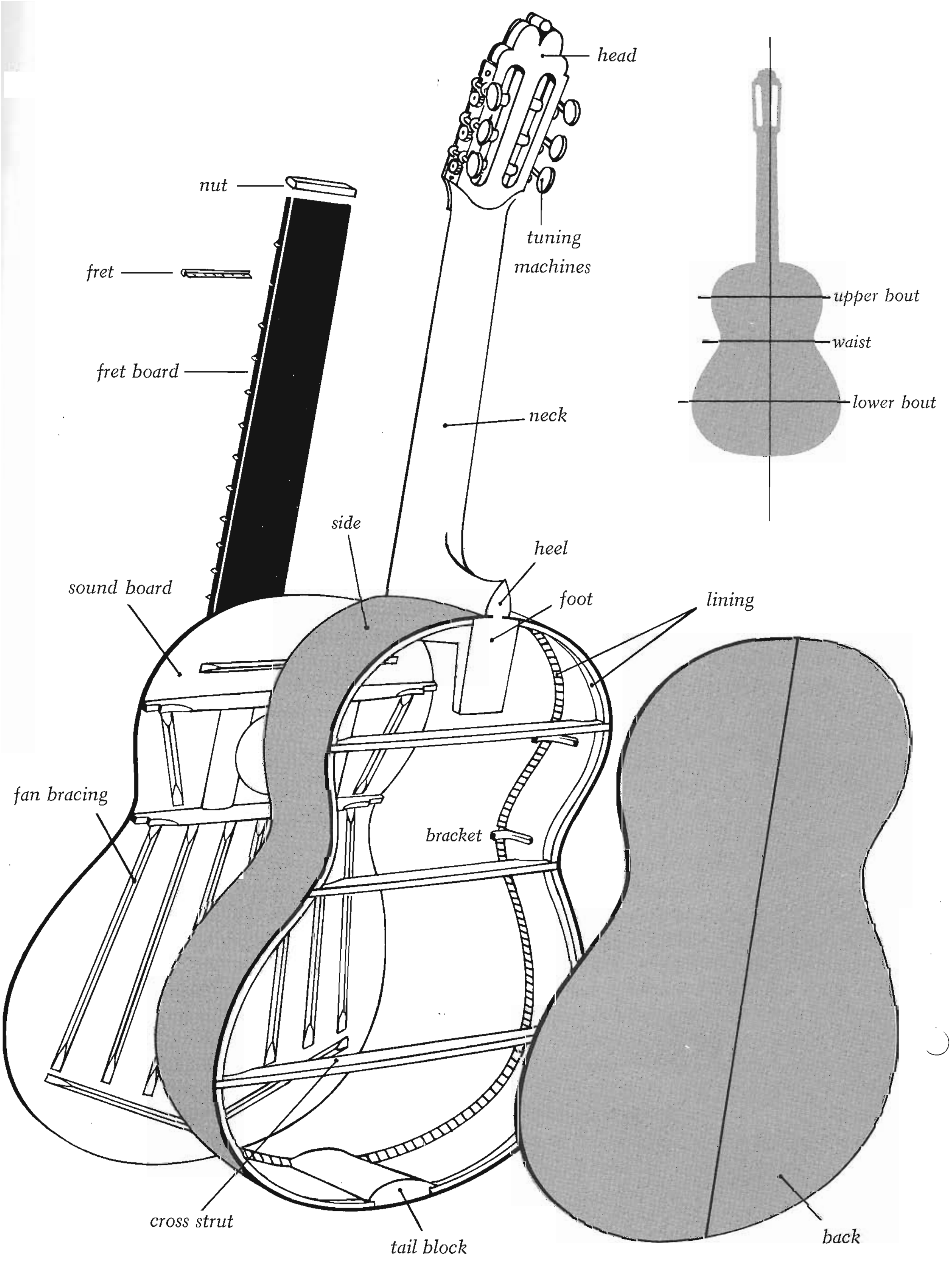
head
nut
fret
tuning
machines
upper bout
waist
lower bout
fret board
neck
side
heel
sound board
foot
lining
fan bracing
bracket
cross strut
tail block
back

Figure 2.1: Exploded view of a classical guitar, from [37].

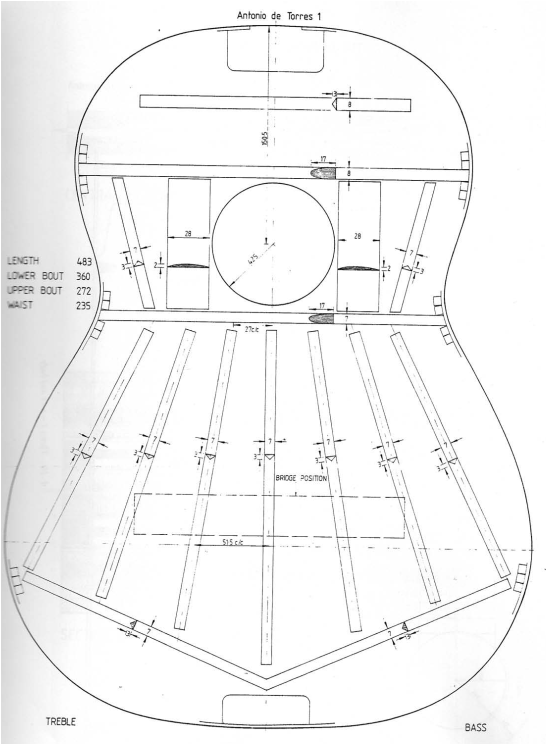
Antonio de Torres 1
LENGTH 483
LOWER BOUT 360
UPPER BOUT 272
WAIST 235
150.5
17
8
28
42.5
27c/c
BRIDGE POSITION
51.5 c/c
TREBLE
BASS

Figure 2.2: Soundboard drawing used as a reference, from [35]. This is in turn modeled after a Torres guitar from 1864. All the dimensions in the figure are in mm.

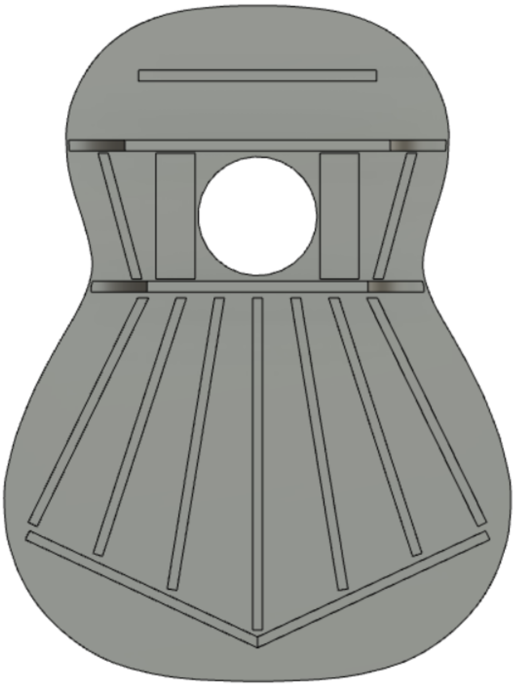

Figure 2.3: Bottom view of the soundboard model with the bracing.

2.1.3. Back

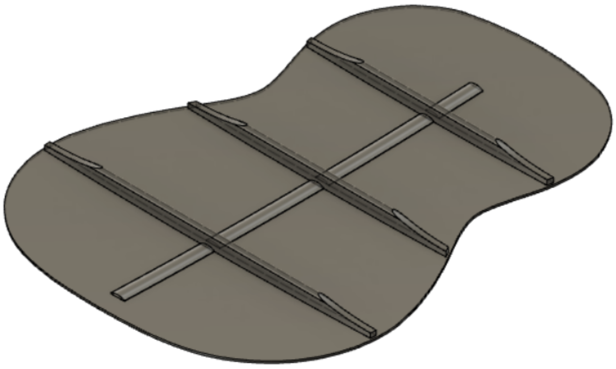

Figure 2.4: Model of the back plate, showing the three transverse braces, and the reinforcing strip.

The back was modeled with a thickness of 2 mm and a spherical arching of $16'$ (=4.8768 m). The arching is offset towards the lower bout, so that the soundbox is deeper at the tail than at the heel.

Three transverse bars were added, as well as a reinforcing strip. The latter runs along the main axis of the instrument, and it is meant to reinforce the joint between the two book-matched pieces that compose the plate. It is 15 mm wide and 3 mm thick.

The back braces, on the other hand, are meant to add rigidity to the back in the transverse direction. They are 6 mm wide and 15 mm thick, and they have a rounded profile and scalloped ends.

2.1.4. Ribs, tail block and heel block

The ribs are also 2 mm thick; their height at the tail is 94 mm, while their height at the heel is 88 mm.

Two reinforcing blocks are placed at the joints between the ribs. The tail block is 20x18 mm in section; the heel block is 20x80 mm at the top, and it tapers towards the bottom, where it curves into a horizontal piece over that extends towards the joint strip. The models of the tail and heel blocks and of the ribs can be seen, assembled with the back plate in Fig. 2.5.

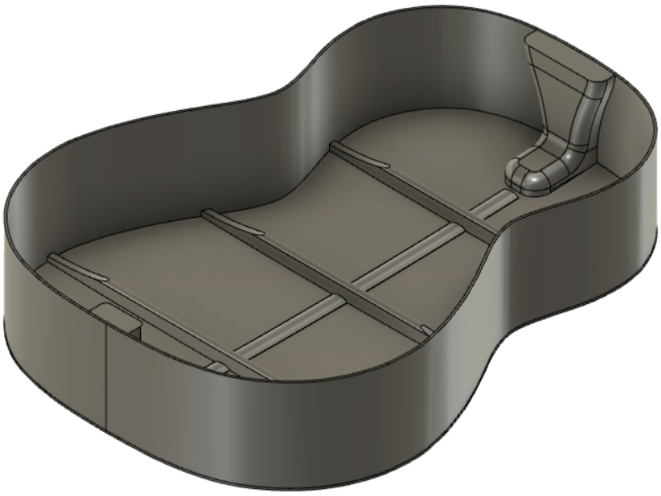

Figure 2.5: Model of the ribs and blocks, assembled over the back plate.

2.1.5. Bridge

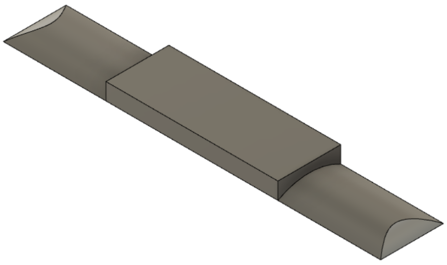

Figure 2.6: Model of the bridge.

A simplified model of the bridge has also been included for the stationary simulations aimed at studying the deformation of the top plate under the tension of the strings. Here the bridge design has been reduced to a rectangular block with two rounded arms on each side, as seen in Fig. 2.6.

2.2. Parametric Model of the metamaterial top

The reference models of the soundboard and of the complete body designed with Autodesk Fusion 360® have then been exported as STEP files. The finite element simulations in this work are all performed with the COMSOL Multiphysics® software [38], as detailed in Chapter 3; this software, however, also has built-in CAD capabilities. Taking advantage of these features, we used COMSOL software to import the STEP file of the reference

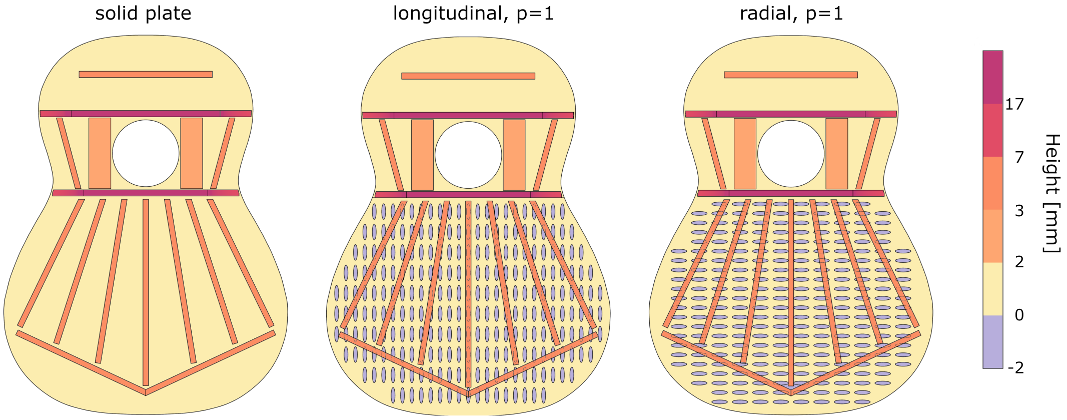

Figure 2.7: Diagram showing the underside of the solid top plate, as well as those with longitudinal (left) and radial (right) holes. The arrows show the directions of the longitudinal (L) and radial (R) axes of the plate's wood. The colors mark the height of each surface with respect to the lower surface of the plate.

guitar model, and to modify it by generating parametrically the patterns of perforations in the guitar's top plate that are the main object of study of the present thesis. This allowed us to perform parametric sweeps in COMSOL that let us launch simulations over many different choices of hole patterns with a single command, simplifying the workflow. The hole patterns are generated by juxtaposition of several copies of the same unitary cell (see Fig. 2.8) over the lower bout of the soundboard. The cell is rectangular, with a size of 26×12 mm for all simulations, but we distinguish between two kinds of holes based on its orientation: here and throughout the rest of this work, when the long side is parallel to the longitudinal axis of the soundboard's wood, we'll talk about *longitudinal* holes, while when it's aligned with the radial axis, we will talk about *radial* holes. The choice of these two orientations has the aim of studying whether the effect of changing the angle of the holes on the effective mechanical properties of wooden plates, observed in [10], would translate to the finished instrument.

The holes themselves are elliptical in shape, and they are centered with respect to the cell. In the reference cell (Fig. 2.8), the semi-major axis a is 10 mm long, while the semi-minor axis b is 2.5 mm long. The size of the holes is changed via a single parameter $p \leq 1$ that scales both a and b simultaneously, keeping the aspect ratio fixed.

Finally, the modification of the soundboard is completed by carving the holes in the underside of the plate by extruding the ellipses to a depth of 2 mm and deleting the intersections between the resulting extrusions and the soundboard.

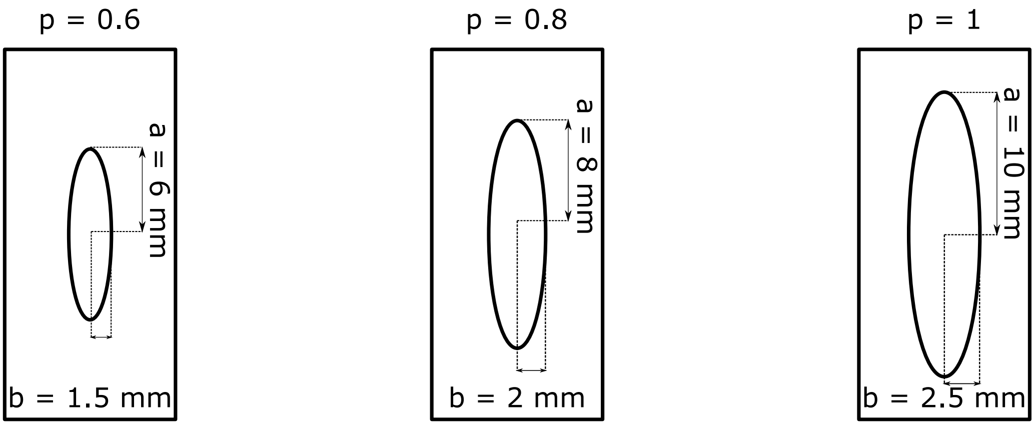

Figure 2.8: Unit cells with three different hole sizes. The hole size is varied with a scaling parameter $p \leq 1$, while both the aspect ratio of the holes and the size of the cell are kept constant.

2.3. Wood choice and mechanical properties

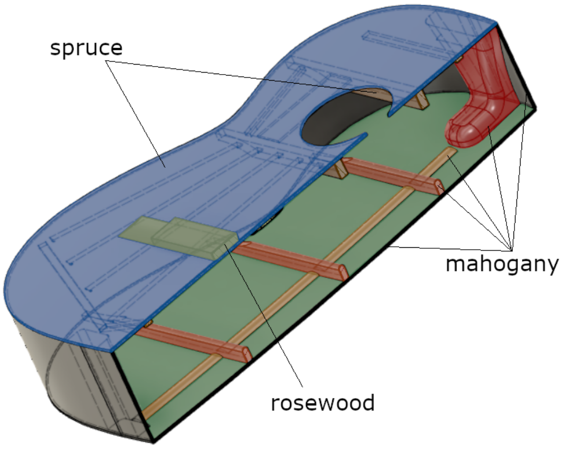

Figure 2.9: 3D cut view of the model of the instrument's body, showing all the individual components and the material that was chose for the main parts.

Several wood species have historically been used in guitar making, with choices varying depending on the time of manufacture, on location, on wood availability and on the particular instrument's intended use. Although red cedar is also widely adopted, the traditional choice for classical guitar soundboards is spruce. Among the wide variety of wood species that exist, spruce is one of those that exhibit the best combinations of high stiffness and low density, while still being strong enough to withstand the tension of the strings [1]. This makes it an excellent choice for the principal sound producing component of the guitar. Traditionally, spruce for guitar soundboards would be sourced from Central Europe;

however, measurements on average material properties for North American varieties are more readily available [13], so we used data for Engelmann spruce (*Picea engelmannii*), which is also commonly used in classical guitars [35]. We used the same material for the braces and the harmonic bars in the top too.

For the back plate and the ribs many choices are available: for instance, cypress is common, especially in flamenco guitars, and maple, while out of fashion in contemporary guitars, has occasionally been used in the past. However, the favourite choice for concert guitars is by far rosewood, both the Brazilian (*Dalbergia nigra*) and East Indian (*Dalbergia latifolia*) types. Despite this, due to a lack of data regarding properties in the directions perpendicular to the longitudinal axis we have decided not to use rosewood for the back and sides, and to use another species which is also a common choice for these components, mahogany. This material is also used for the back braces. Rosewood is still used for the bridge, and its tranverse properties are approximated to be analogous to those observed in other species [39].

Apart from this exception, all material properties are taken from [13], and their values are reported in Table 2.1. The choices of materials for the components of the instrument are also illustrated in Fig. 2.9, alongside a 3D cut view of the instrument's body.

Density [kg m^{-3}]			
Spruce	350		
Mahogany	450		
Rosewood	609		
Young's Moduli [GPa]			
	E_L	E_R	E_T
Spruce	9.79	1.253	0.578
Mahogany	10.12	1.083	0.648
Rosewood	15.8	1.64	0.820
Shear Moduli [GPa]			
	G_{LR}	G_{RT}	G_{LT}
Spruce	1.214	0.0979	1.1748
Mahogany	0.668	0.283	0.870
Rosewood	1.52	0.351	1.52
Poissons's Ratios			
	ν_{LR}	ν_{RT}	ν_{LT}
Spruce	0.422	0.530	0.462
Mahogany	0.314	0.600	0.533
Rosewood	0.3	0.35	0.35

Table 2.1: Properties of the materials chosen for the simulations. For each of the materials we define 9 constants, which, as explained in Chapter 1, are enough to completely characterize its elastic behaviour.

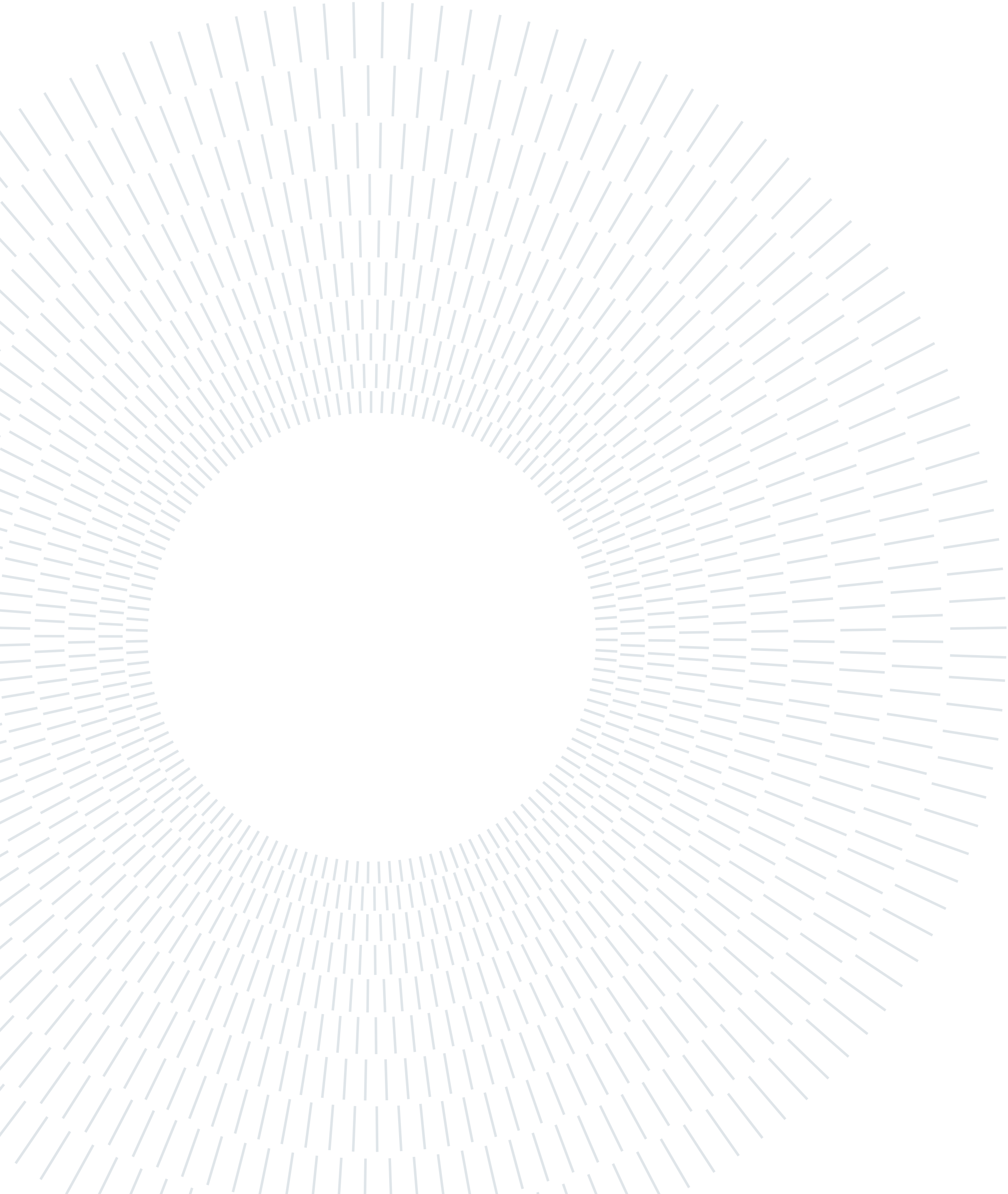

3 Finite Element Analysis of the Guitar

In this chapter, we describe the simulations that were performed with the numerical model of the guitar and present their results. These simulations represent an exploration of the effect of the use of wooden metamaterials in the finished instrument on its mechanical behavior. First, a modal analysis of the soundboards in free boundary conditions and of the complete guitar bodies is presented, comparing the natural modes and frequencies for the different choices of holes with those for the solid top and with each other. Next, we describe a series of stationary simulations aimed at studying the deformation of the soundboard under the tension of the strings. Finally, we report on the frequency domain simulations which were conducted in order to evaluate the driving point mobility of the instrument's body in the area under the bridge.

3.1. FE Analysis in COMSOL Multiphysics®

The finite element simulations were all performed with COMSOL Multiphysics® software [38]. As already explained in Chapter 2, the models of the soundboard and of the complete instrument designed with Fusion 360® were imported in COMSOL and, when needed, modified with the desired hole patterns for the simulations. The elastic constants of the materials were then properly specified as detailed in Section 2.3, taking care of defining correctly the directions of the principal axes for all the components. The models were discretized with 3D solid elements, using the Solid Mechanics interface from COMSOL's Structural Mechanics Module [40]. The mesh was generated by the software using a mixture of unstructured free tetrahedral mesh parts and structured swept mesh parts (both from triangular and quadrilateral surface meshes).

3.2. Eigenfrequency simulations for modal analysis

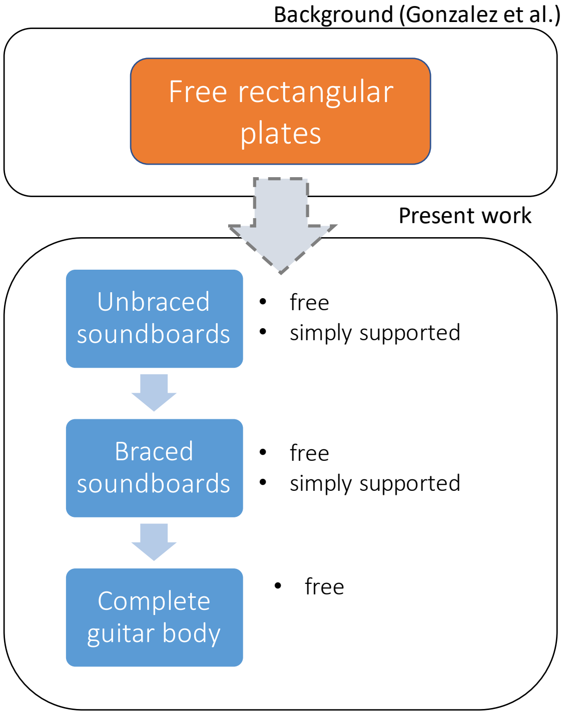
Background (Gonzalez et al.)
Free rectangular plates
Present work
Unbraced soundboards
• free
• simply supported
Braced soundboards
• free
• simply supported
Complete guitar body
• free

Figure 3.1: Diagram of the workflow for the eigenfrequency simulations. The results in [10] have been obtained by studying the modal behavior of free rectangular plate. To investigate possible applications to guitar soundboards, we performed eigenfrequency studies on the soundboard by incrementally adding elements, increasing the complexity of the structure from the free unbraced plate toup to the complete body of the instrument.

The first studies that were performed are a series of eigenfrequencies simulations, aimed at characterizing the vibrational behavior of the soundboard and of the instrument through modal analysis. We focused our attention at first on the metamaterial soundboards alone, with and without braces, both in free and simply supported boundary conditions, and then applied the same analysis to the complete body of the instruments. A diagram illustrating the workflow has been reported in Fig. 3.1. We seek not only to gain insight into the effect of the metamaterial on the mechanics of the soundboard, but also into how they compare to those introduced by the addition of the braces and the interaction with the ribs and the back plate.

3.2.1. Modal analysis of the free, unbraced plates

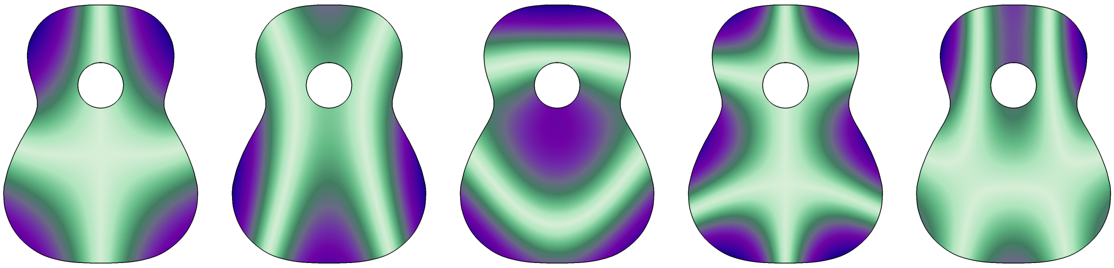

Figure 3.2: Mode shapes of the unbraced solid soundboard in free boundary conditions for the 5 lowest eigenfrequencies, in ascending order from left to right.

First of all, eigenfrequency simulations were performed with the unbraced soundboard in free boundary conditions. The first 12 eigenfrequencies and corresponding modal shapes were computed for various hole sizes, both with radial and longitudinal orientation, and the results were compared to those obtained for the solid soundboard (without perforations). The modal shapes corresponding to the 5 lowest eigenfrequencies of the solid plate can be seen in Fig. 3.2. Fig. 3.3 shows the computed eigenfrequencies with longitudinal (p=1) and radial (p=1) holes as well as those of the solid plate. The effect, overall, appears to be a slight decrease in the value of the eigenfrequencies, more accentuated in the case of the radial holes. This trend is confirmed by Fig. 3.4, which shows the percentage variation of the eigenfrequencies relative to the solid plate, for all the choices of hole size and orientation that were simulated. In most cases, we observe lowering of the frequencies, an effect which is strengthened with increasing hole size, and appears more pronounced for the radial holes. Another interesting effect is revealed by the variation of the frequencies for modes 2 and 3. These are related to the fundamental cross grain and long grain modes for a free rectangular wooden plate, whose frequencies are respectively proportional to $\sqrt{E_R}$ and $\sqrt{E_L}$ [41]. We expect the frequencies of modes 2 and 3 of the

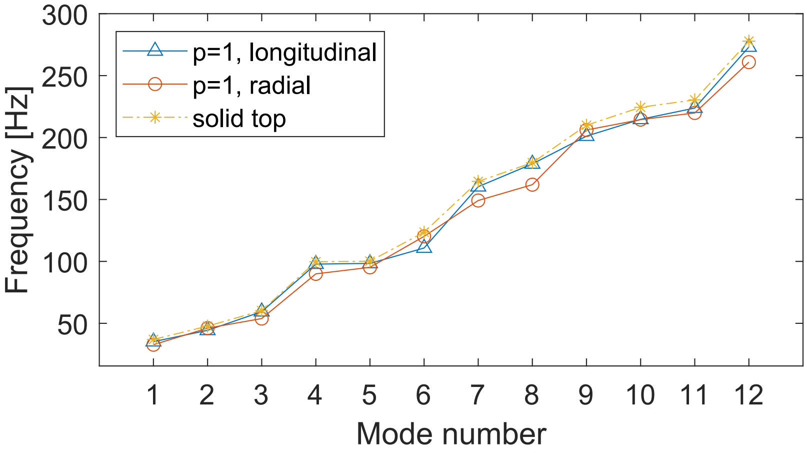

Figure 3.3: First 12 eigenfrequencies for the free, unbraced soundboard, with longitudinal holes (p=1), radial holes (p=1) and in the case of the solid plate.

free unbraced soundboard to be similarly related to its effective elastic moduli, so we can gain insight into the effect of the different hole sizes and orientation on these parameters. For mode 2, we can see how the variation is more pronounced in the case of the longitudinal holes (-7.1% for $p = 1$) than the case of the radial holes (-3.4% for $p = 1$). This points to sharper decrease in the effective value of E_R with longitudinal holes compared to the radial holes. Conversely, for mode 3 we see the opposite effect, with an even starker contrast: with longitudinal holes the frequency is only slightly lowered (-1.4% for $p = 1$), while there is a significant decrease with radial holes (-10.6% with p=1). In turn, this points to a more pronounced decrease in the effective value of E_L in the case of the radial holes, compared to the longitudinal holes. Notably, this is the same trend observed in rectangular wooden plates in [10].

The modal shapes are compared with the Modal Assurance Criterion (MAC)[42], a widely used indicator which offers a quantitative measure of consistency between pairs of modal vectors. Fig. 3.5 shows the matrices of the MAC coefficients comparing the modes of the plates with longitudinal (p=1) and radial (p=1) holes with the modes of the solid plate. It's immediately apparent that most modal shapes are not significantly modified by the introduction of the metamaterial, since we have values close to unity in the diagonal, and close to zero outside. The only deviation in the case of the longitudinal holes appears for modes 9 and 10; however, given the high values of the coefficients (9,10) and (10,9),

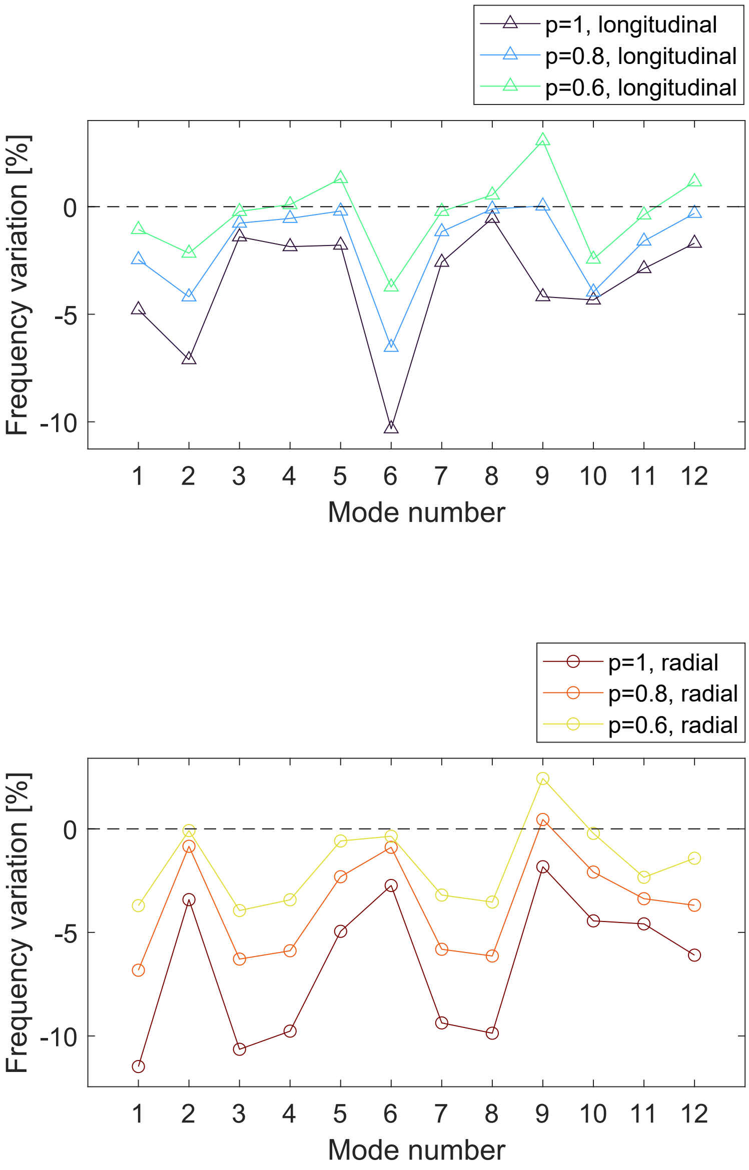

Figure 3.4: Percentage variation of the eigenfrequencies for the unbraced plates in free boundary conditions, with different hole sizes and orientations, with respect to the eigenfrequencies of the solid plate.

this appears to be a simple mode switch i. e. a case where the eigenfrequencies of two modes cross each other changing the ordering of the mode pair. For the radial holes we have a slightly more complex situation for what concerns modes 9, 10 and 11. First of all, mode 9 of the metamaterial plate still appears mostly correlated to mode 9 of the solid plate, but with coefficient (9,9) being ~ 0.6 and coefficients (9,10) and (11,9) being ~ 0.3, it's evident that the modal shape has been modified to a significant degree. For

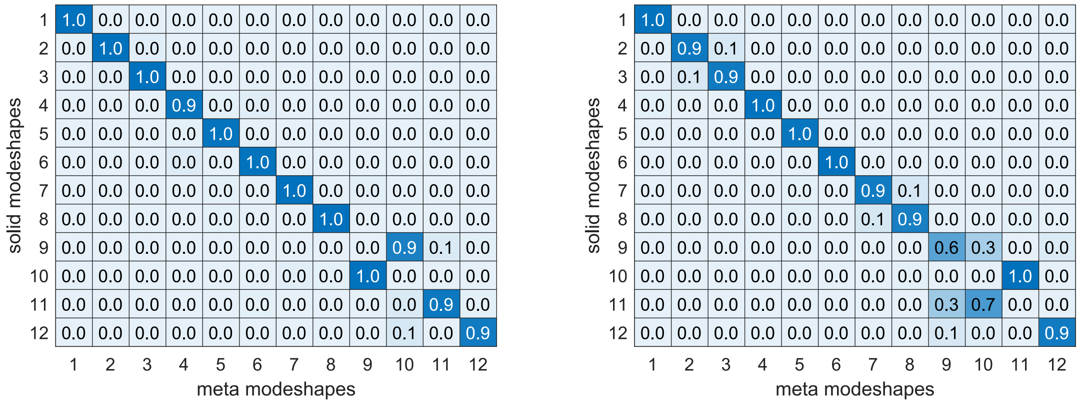
solid modeshapes
meta modeshapes
solid modeshapes
meta modeshapes

	1	2	3	4	5	6	7	8	9	10	11	12
1	1.0	0.0	0.0	0.0	0.0	0.0	0.0	0.0	0.0	0.0	0.0	0.0
2	0.0	1.0	0.0	0.0	0.0	0.0	0.0	0.0	0.0	0.0	0.0	0.0
3	0.0	0.0	1.0	0.0	0.0	0.0	0.0	0.0	0.0	0.0	0.0	0.0
4	0.0	0.0	0.0	0.9	0.0	0.0	0.0	0.0	0.0	0.0	0.0	0.0
5	0.0	0.0	0.0	0.0	1.0	0.0	0.0	0.0	0.0	0.0	0.0	0.0
6	0.0	0.0	0.0	0.0	0.0	1.0	0.0	0.0	0.0	0.0	0.0	0.0
7	0.0	0.0	0.0	0.0	0.0	0.0	1.0	0.0	0.0	0.0	0.0	0.0
8	0.0	0.0	0.0	0.0	0.0	0.0	0.0	1.0	0.0	0.0	0.0	0.0
9	0.0	0.0	0.0	0.0	0.0	0.0	0.0	0.0	0.0	0.9	0.1	0.0
10	0.0	0.0	0.0	0.0	0.0	0.0	0.0	0.0	1.0	0.0	0.0	0.0
11	0.0	0.0	0.0	0.0	0.0	0.0	0.0	0.0	0.0	0.0	0.9	0.0
12	0.0	0.0	0.0	0.0	0.0	0.0	0.0	0.0	0.0	0.1	0.0	0.9

	1	2	3	4	5	6	7	8	9	10	11	12
1	1.0	0.0	0.0	0.0	0.0	0.0	0.0	0.0	0.0	0.0	0.0	0.0
2	0.0	0.9	0.1	0.0	0.0	0.0	0.0	0.0	0.0	0.0	0.0	0.0
3	0.0	0.1	0.9	0.0	0.0	0.0	0.0	0.0	0.0	0.0	0.0	0.0
4	0.0	0.0	0.0	1.0	0.0	0.0	0.0	0.0	0.0	0.0	0.0	0.0
5	0.0	0.0	0.0	0.0	1.0	0.0	0.0	0.0	0.0	0.0	0.0	0.0
6	0.0	0.0	0.0	0.0	0.0	1.0	0.0	0.0	0.0	0.0	0.0	0.0
7	0.0	0.0	0.0	0.0	0.0	0.0	0.9	0.1	0.0	0.0	0.0	0.0
8	0.0	0.0	0.0	0.0	0.0	0.0	0.1	0.9	0.0	0.0	0.0	0.0
9	0.0	0.0	0.0	0.0	0.0	0.0	0.0	0.0	0.6	0.3	0.0	0.0
10	0.0	0.0	0.0	0.0	0.0	0.0	0.0	0.0	0.0	0.0	1.0	0.0
11	0.0	0.0	0.0	0.0	0.0	0.0	0.0	0.0	0.3	0.7	0.0	0.0
12	0.0	0.0	0.0	0.0	0.0	0.0	0.0	0.0	0.1	0.0	0.0	0.9

Figure 3.5: Matrices of the MAC coefficients between the modal shapes of the free, unbraced metamaterial soundboards, and the modal shapes of the solid plate. On the left the matrix for the case of the longitudinal holes (p=1), on the right the one for the case of the radial holes (p=1).

what concerns modes 10 and 11, then, we can identify a mode switch, but given a value of ~ 0.7 for coefficient (11,10), plus the non-negligible values of coefficients (9,10) and (11,9), we can conclude that here too the modal shape has changed conspicuously.

3.2.2. Modal analysis of the unbraced plates in simply supported boundary conditions

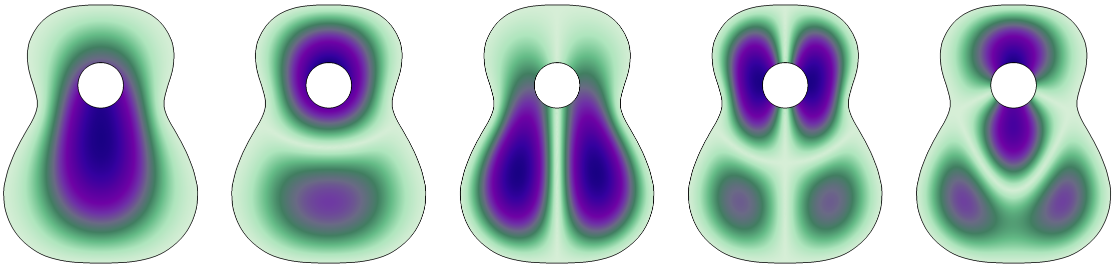

Figure 3.6: Mode shapes of the unbraced solid soundboard in simply supported boundary conditions for the 5 lowest eigenfrequencies.

The very same studies were conducted for the unbraced plate in simply supported boundary conditions as well. These boundary conditions, for 2D plates, impose zero vertical displacement and zero bending moment at the boundaries. However, since we used a discretization with 3D solid elements, these conditions had to be replicated indirectly. The approach we used was to impose a fixed constraint on the outer edge of the lower surface of the soundboard. Movement of this edge is thus prevented, constraining the vertical displacement of the plate, while still allowing free bending rotation at the plate's sides. This situation is closer to that of the soundboard attached to the ribs of the finished instrument than the case of the free plate (even though the actual boundary conditions are somewhere in between simply supported and clamped [43]). Fg. 3.6 shows the first 5 eigenmodes of the solid plate with these boundary conditions, while Fig. 3.7 shows the computed eigenfrequencies in the cases of the solid plate, of the longitudinal holes ($p = 1$) and radial holes ($p = 1$). As expected, the introduction of the boundary conditions raises the values of the eigenfrequencies. As for the variation introduced by the metamaterials, a separation in the observed effects seems to be introduced by the orientation of the holes. As shown in Fig. 3.8, where the percentage variations in the eigenfrequencies are reported, most values are lowered in the case of the radial holes, and the largest the size of the holes, the more significant the decrease. On the other hand, with longitudinal holes the variations are both less one-sided, with many of the eigenfrequencies having been raised, and smaller in absolute terms. Here too, however, increasing hole size appears to be correlated, for most frequencies, to a lowering of the values.

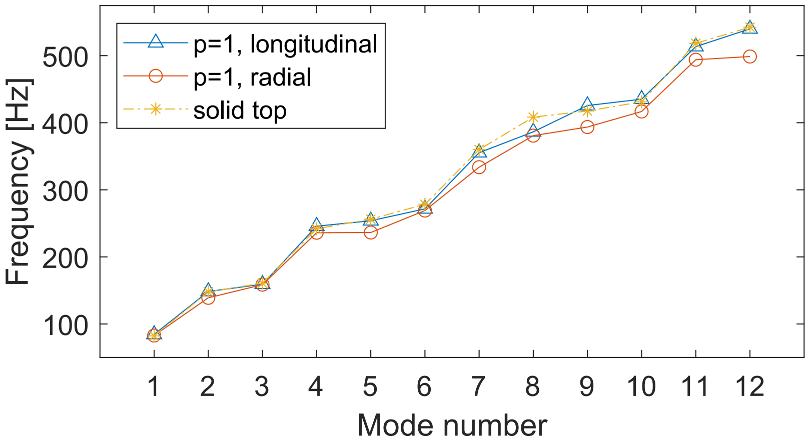

Figure 3.7: First 12 eigenfrequencies for the unbraced soundboard in simply supported boundary conditions, with longitudinal holes (p=1), radial holes (p=1) and in the case of the solid plate.

The modal shapes have also been compared with the MAC. The computed values of the MAC coefficients comparing the modes of plates with longitudinal ($p = 1$) and radial ($p = 1$) holes to those of the solid plate are reported in Fig. 3.9. The matrix for the

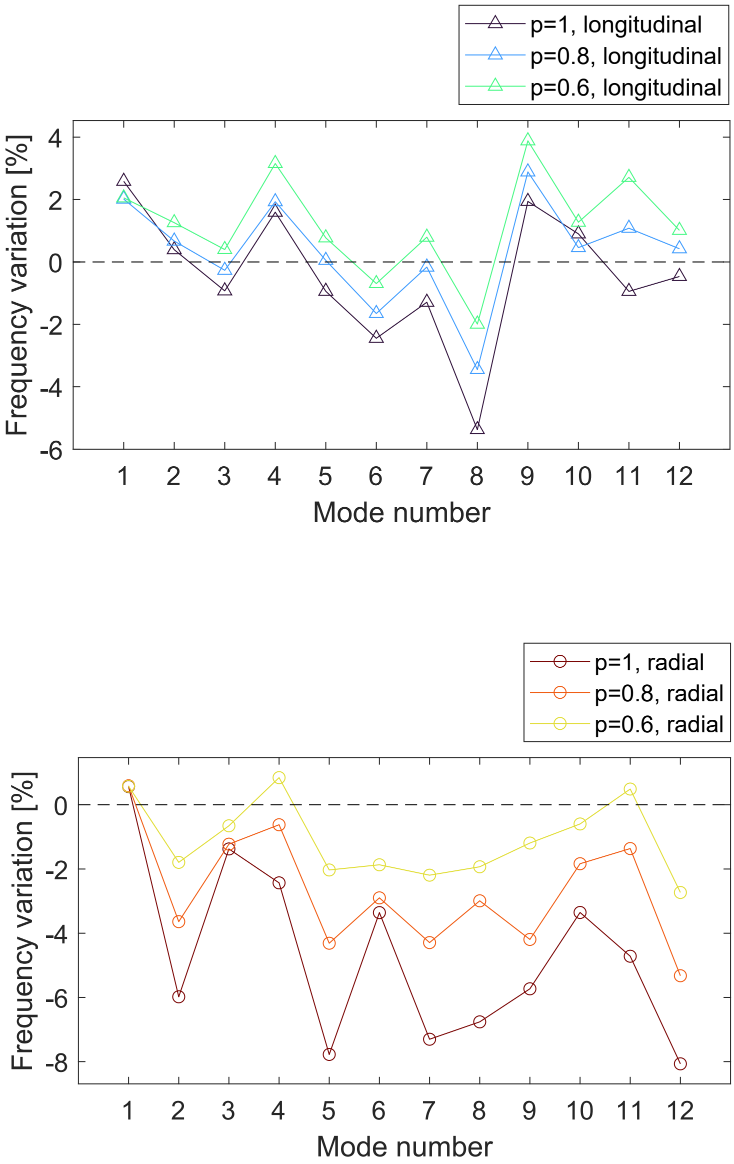

Figure 3.8: Percentage variation of the eigenfrequencies for the unbraced plates in simply supported boundary conditions, with different hole sizes and orientations, with respect to the eigenfrequencies of the solid plate.

longitudinal holes shows fairly high values on the diagonal and low values outside for the first 8 modes, while the mode shapes for higher modes present more significant changes. For the radial holes, we can identify a mode switch between modes 4 and 5, as well as modes 11 and 12. Interestingly, modes 8, 9 and 10 seem to undergo a three-way mode switch, where mode 8 in the metamaterial plate is similar to mode 10 of the solid plate, mode 9 of the metamaterial plate is similar to mode 8 of the solid plate, and mode 10 of the metamaterial plate is similar to mode 9 of the solid plate.

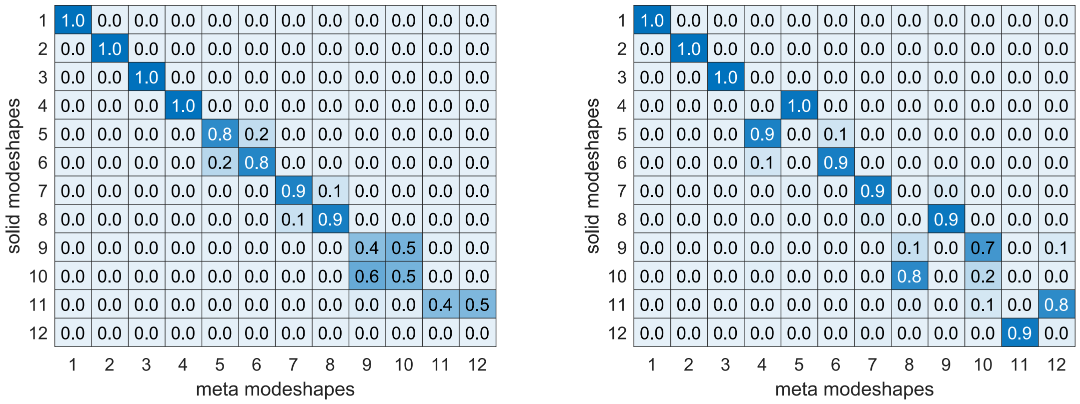

	1	2	3	4	5	6	7	8	9	10	11	12
1	1.0	0.0	0.0	0.0	0.0	0.0	0.0	0.0	0.0	0.0	0.0	0.0
2	0.0	1.0	0.0	0.0	0.0	0.0	0.0	0.0	0.0	0.0	0.0	0.0
3	0.0	0.0	1.0	0.0	0.0	0.0	0.0	0.0	0.0	0.0	0.0	0.0
4	0.0	0.0	0.0	1.0	0.0	0.0	0.0	0.0	0.0	0.0	0.0	0.0
5	0.0	0.0	0.0	0.0	0.8	0.2	0.0	0.0	0.0	0.0	0.0	0.0
6	0.0	0.0	0.0	0.0	0.2	0.8	0.0	0.0	0.0	0.0	0.0	0.0
7	0.0	0.0	0.0	0.0	0.0	0.0	0.9	0.1	0.0	0.0	0.0	0.0
8	0.0	0.0	0.0	0.0	0.0	0.0	0.1	0.9	0.0	0.0	0.0	0.0
9	0.0	0.0	0.0	0.0	0.0	0.0	0.0	0.0	0.4	0.5	0.0	0.0
10	0.0	0.0	0.0	0.0	0.0	0.0	0.0	0.0	0.6	0.5	0.0	0.0
11	0.0	0.0	0.0	0.0	0.0	0.0	0.0	0.0	0.0	0.0	0.4	0.5
12	0.0	0.0	0.0	0.0	0.0	0.0	0.0	0.0	0.0	0.0	0.0	0.0

	1	2	3	4	5	6	7	8	9	10	11	12
1	1.0	0.0	0.0	0.0	0.0	0.0	0.0	0.0	0.0	0.0	0.0	0.0
2	0.0	1.0	0.0	0.0	0.0	0.0	0.0	0.0	0.0	0.0	0.0	0.0
3	0.0	0.0	1.0	0.0	0.0	0.0	0.0	0.0	0.0	0.0	0.0	0.0
4	0.0	0.0	0.0	0.0	1.0	0.0	0.0	0.0	0.0	0.0	0.0	0.0
5	0.0	0.0	0.0	0.9	0.0	0.1	0.0	0.0	0.0	0.0	0.0	0.0
6	0.0	0.0	0.0	0.1	0.0	0.9	0.0	0.0	0.0	0.0	0.0	0.0
7	0.0	0.0	0.0	0.0	0.0	0.0	0.9	0.0	0.0	0.0	0.0	0.0
8	0.0	0.0	0.0	0.0	0.0	0.0	0.0	0.0	0.9	0.0	0.0	0.0
9	0.0	0.0	0.0	0.0	0.0	0.0	0.0	0.1	0.0	0.7	0.0	0.1
10	0.0	0.0	0.0	0.0	0.0	0.0	0.0	0.8	0.0	0.2	0.0	0.0
11	0.0	0.0	0.0	0.0	0.0	0.0	0.0	0.0	0.0	0.1	0.0	0.8
12	0.0	0.0	0.0	0.0	0.0	0.0	0.0	0.0	0.0	0.0	0.9	0.0

Figure 3.9: Matrices of the MAC coefficients between the modal shapes of the unbraced metamaterial soundboards in simply supported boundary conditions, and the modal shapes of the solid plate. On the left the matrix for the case of the longitudinal holes (p=1), on the right the one for the case of the radial holes (p=1).

3.2.3. Modal analysis of the free, braced plates

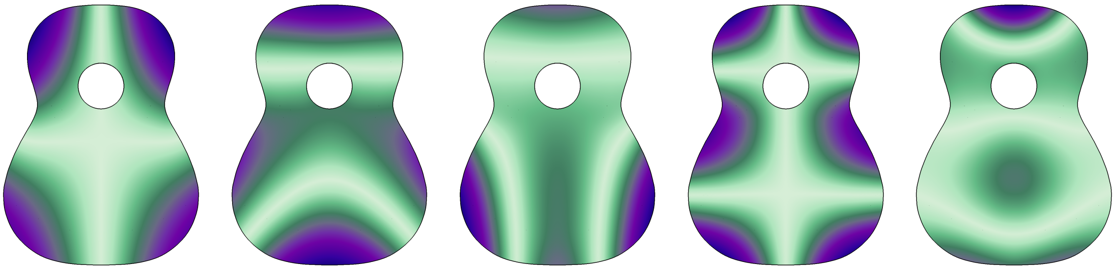

Figure 3.10: Mode shapes of the braced solid soundboard in free boundary conditions for the 5 lowest eigenfrequencies, in ascending order from left to right.

Following the studies on the unbraced soundboards, a study on the modes of the braced soundboard was carried out, in free boundary conditions. Mode shapes for the lowest modes of the solid soundboard are reported in Fig. 3.14. Fig. 3.11 shows a plot of the eigenfrequencies for the cases of the metamaterial plates with the largest holes (p=1) in both orientations, compared with those of the solid plate. The values are increased with respect to the free unbraced plate as a consequence of the extra stiffness introduced by the braces, but they are still slightly lower than those of the unbraced simply supported plate. Overall there seems to be a slight increase for the longitudinal holes and, conversely, a slight decrease for the radial holes. This trend is confirmed by looking at Fig. 3.12, which reports the percentage variation in the eigenfrequencies for all the hole patterns that were simulated. For the radial holes, in particular, all eigenfrequencies are lowered by $\sim 2\%$ or more, the effect being clearly accentuated by increasing the size of the holes. As for the the longitudinal holes, there is an overall increase in the eigenfrequencies with respect to the solid plate, but the trend with increasing hole size is less clear: indeed, the eigenfrequencies are clearly raised with greater hole size only for modes 2, 3, 4 and 6.

The MAC values comparing the modal shapes of the free, braced metamaterial plates with longitudinal (p=1) and radial (p=1) holes with those of the solid plate are reported as a heatmap in Fig. 3.13. It appears evident that there is a strong correlation between the modes in the different frequencies, as all non-null values are close to unity, suggesting that the modal shapes aren't altered significantly. Furthermore, most of these high MAC values lie on the diagonal of the matrices, and those that don't are clearly the result of a mode switch (namely modes 9 and 10 with the radial holes and modes 5 and 6 in both cases).

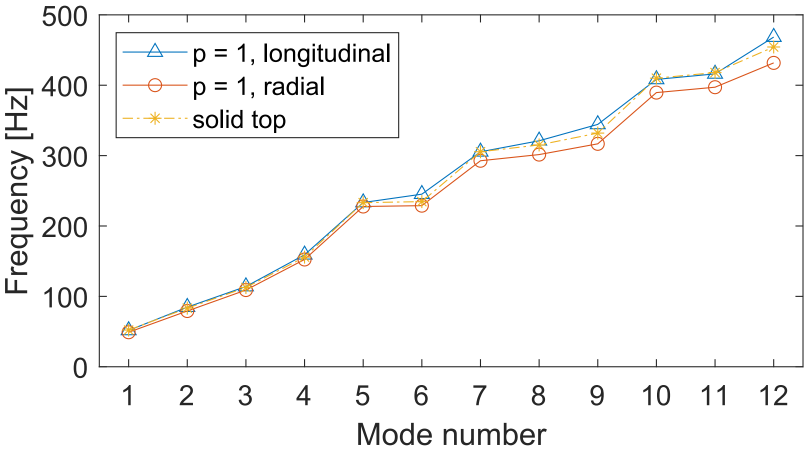

Figure 3.11: First 12 eigenfrequencies for the braced soundboard in free boundary conditions, in three cases: with longitudinal holes (p=1), with radial holes (p=1) and the solid plate.

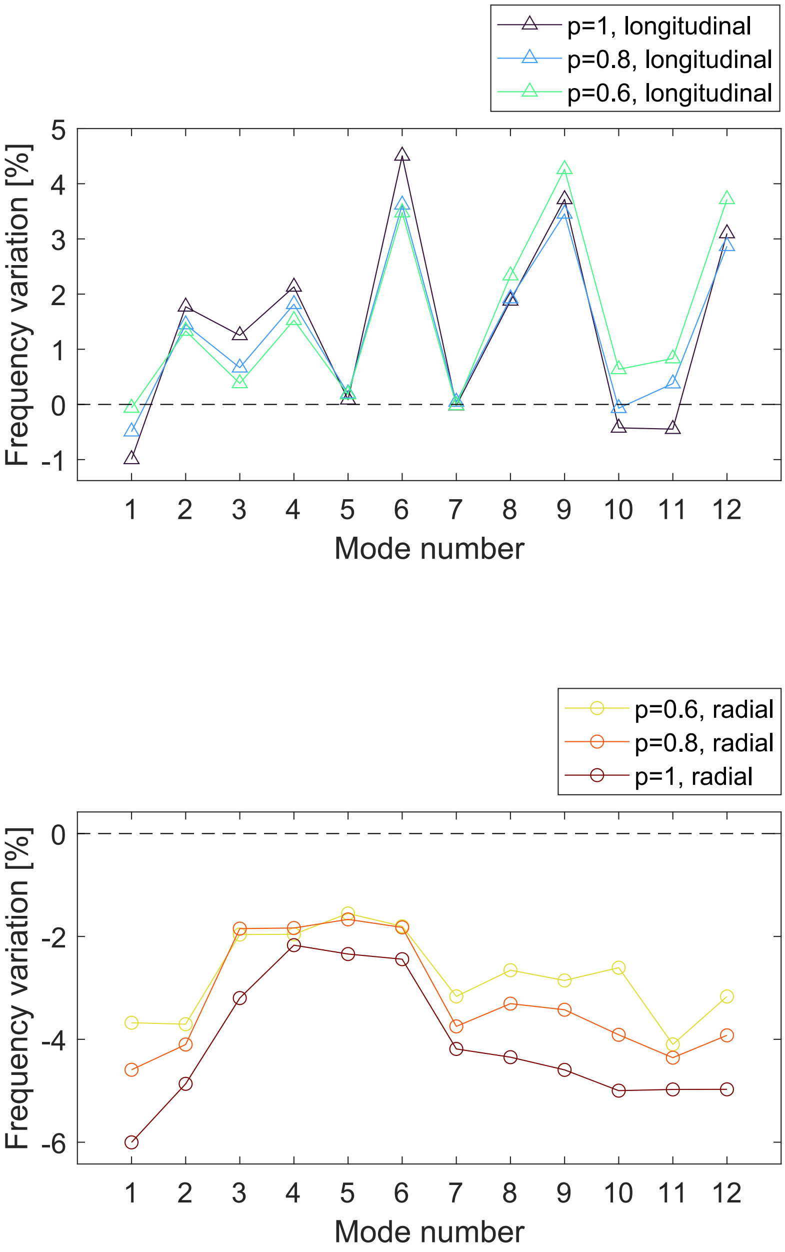

Figure 3.12: Percentage variation of the eigenfrequencies for the braced plates in free boundary conditions, with different hole sizes and orientations, with respect to the eigenfrequencies of the solid plate, in ascending order from left to right.

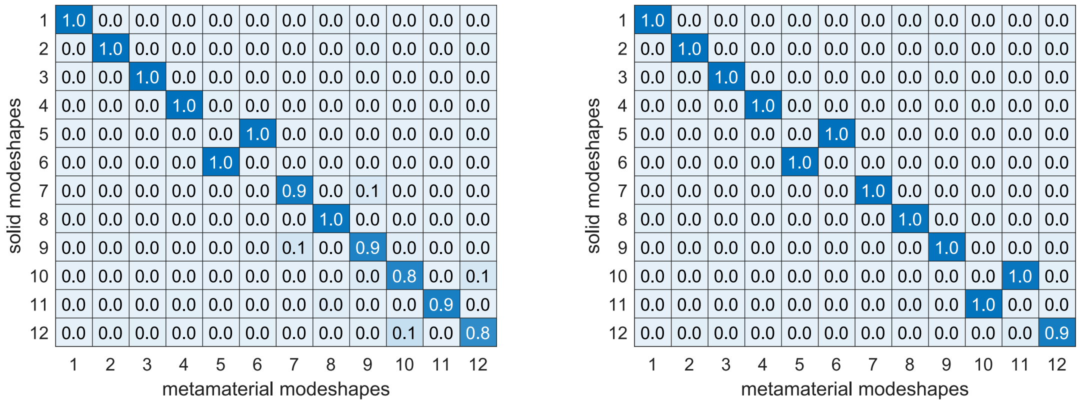

	1	2	3	4	5	6	7	8	9	10	11	12
1	1.0	0.0	0.0	0.0	0.0	0.0	0.0	0.0	0.0	0.0	0.0	0.0
2	0.0	1.0	0.0	0.0	0.0	0.0	0.0	0.0	0.0	0.0	0.0	0.0
3	0.0	0.0	1.0	0.0	0.0	0.0	0.0	0.0	0.0	0.0	0.0	0.0
4	0.0	0.0	0.0	1.0	0.0	0.0	0.0	0.0	0.0	0.0	0.0	0.0
5	0.0	0.0	0.0	0.0	0.0	1.0	0.0	0.0	0.0	0.0	0.0	0.0
6	0.0	0.0	0.0	0.0	1.0	0.0	0.0	0.0	0.0	0.0	0.0	0.0
7	0.0	0.0	0.0	0.0	0.0	0.0	0.9	0.0	0.1	0.0	0.0	0.0
8	0.0	0.0	0.0	0.0	0.0	0.0	0.0	1.0	0.0	0.0	0.0	0.0
9	0.0	0.0	0.0	0.0	0.0	0.0	0.1	0.0	0.9	0.0	0.0	0.0
10	0.0	0.0	0.0	0.0	0.0	0.0	0.0	0.0	0.0	0.8	0.0	0.1
11	0.0	0.0	0.0	0.0	0.0	0.0	0.0	0.0	0.0	0.0	0.9	0.0
12	0.0	0.0	0.0	0.0	0.0	0.0	0.0	0.0	0.0	0.1	0.0	0.8

	1	2	3	4	5	6	7	8	9	10	11	12
1	1.0	0.0	0.0	0.0	0.0	0.0	0.0	0.0	0.0	0.0	0.0	0.0
2	0.0	1.0	0.0	0.0	0.0	0.0	0.0	0.0	0.0	0.0	0.0	0.0
3	0.0	0.0	1.0	0.0	0.0	0.0	0.0	0.0	0.0	0.0	0.0	0.0
4	0.0	0.0	0.0	1.0	0.0	0.0	0.0	0.0	0.0	0.0	0.0	0.0
5	0.0	0.0	0.0	0.0	0.0	1.0	0.0	0.0	0.0	0.0	0.0	0.0
6	0.0	0.0	0.0	0.0	1.0	0.0	0.0	0.0	0.0	0.0	0.0	0.0
7	0.0	0.0	0.0	0.0	0.0	0.0	1.0	0.0	0.0	0.0	0.0	0.0
8	0.0	0.0	0.0	0.0	0.0	0.0	0.0	1.0	0.0	0.0	0.0	0.0
9	0.0	0.0	0.0	0.0	0.0	0.0	0.0	0.0	1.0	0.0	0.0	0.0
10	0.0	0.0	0.0	0.0	0.0	0.0	0.0	0.0	0.0	0.0	1.0	0.0
11	0.0	0.0	0.0	0.0	0.0	0.0	0.0	0.0	0.0	1.0	0.0	0.0
12	0.0	0.0	0.0	0.0	0.0	0.0	0.0	0.0	0.0	0.0	0.0	0.9

Figure 3.13: MAC matrices comparing the modal shapes of the free, braced metamaterial soundboards with those of the solid one. On the left the matrix for the case of the longitudinal holes (p=1), on the right the one for the case of the radial holes (p=1).

3.2.4. Modal analysis of the braced plates in simply supported boundary conditions

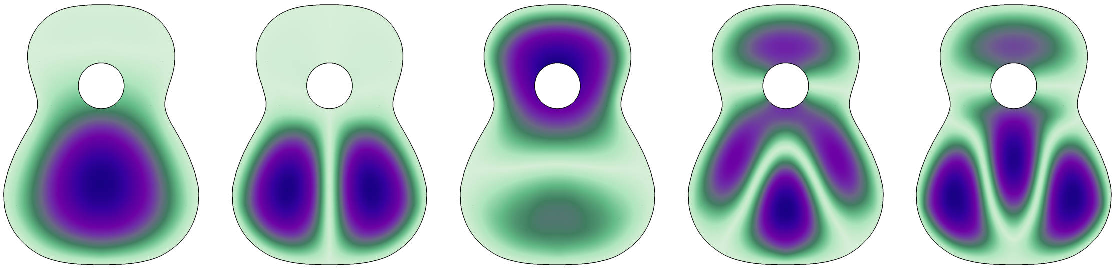

Figure 3.14: Mode shapes of the braced solid soundboard in simply supported boundary conditions for the 5 lowest eigenfrequencies.

Once again, the same kind of analysis we have described so far was applied to the braced soundboards with simply supported boundary conditions. We notice, first of all, that the values of the eigenfrequencies, reported in Fig. 3.15, are significantly higher than those of the free, braced soundboard. This is an expected effect of the imposition of these boundary conditions. It's also clear that the variations are even smaller than in the aforementioned case. This behavior seems to be confirmed by looking at the percentage variations, reported in Fig. 3.16. Notice how this time, while there seem to be clear trends with varying hole size for some of the eigenfrequencies, it's not really possible to identify an overall upwards or downwards shift with either longitudinal or radial holes.
The comparison of the modal shapes obtained with the MAC, the values of which are shown in Fig. 3.17, seems to also show little variation between metamaterial plates and the solid one. In the case of the radial holes (p=1), the MACs are close to unity on the diagonal and very low elsewhere, indicating that the modal shapes are almost unaltered. For the radial holes, the situation is very similar, except for a mode switch between modes 9 and 10, and low MAC values for the 12th modes.

3.2.5. Modal analysis of the complete body

Finally, the same kind of simulations performed on the soundboard so far has been applied to the complete model of the guitar body (without the bridge). Fig. 3.19 shows the first 12 eigenfrequencies for the cases of the metamaterial tops with the largest holes in both orientations, as well as those computed for the case of the solid top. Very little difference in the eigenfrequencies between these instances can be appreciated from this graph. Indeed, the variation in the eigenfrequencies is overall the smallest observed so far: from the graph in Fig. 3.20, which shows the percentage difference in the frequencies relative to the body

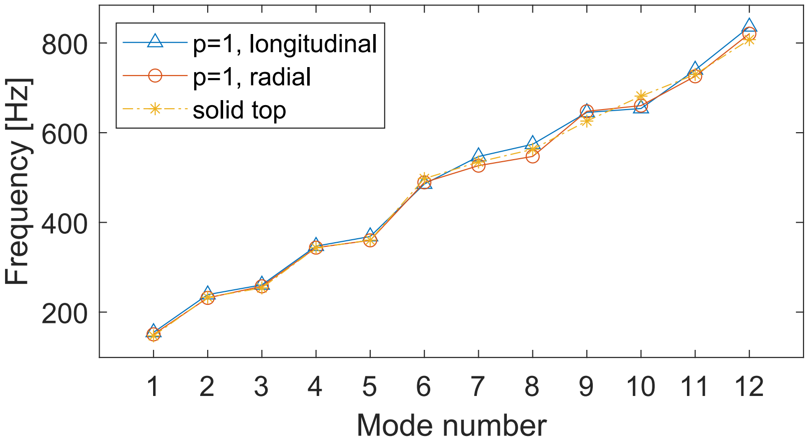

Figure 3.15: First 12 eigenfrequencies for the braced soundboard in simply supported boundary conditions, in three cases: with longitudinal holes (p=1), with radial holes (p=1), and with the solid top.

with the solid top, we can see that there is no case where we have variations greater than 3%.

Very little difference is also observed in the modal shapes, when comparing them with MAC, as shown in Fig. 3.21. Apart from a mode switch between modes 10 and 11 in the case of the longitudinal holes (p=1), the matrices appear pretty much diagonal. The diagonal coefficient for mode 12 in the same case, however, is quite low, indicating a significant change in the corresponding modal shape.

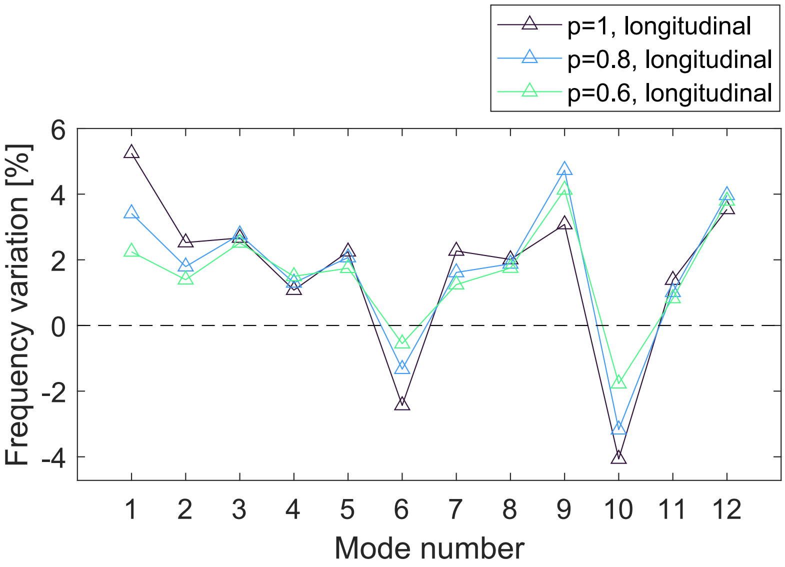

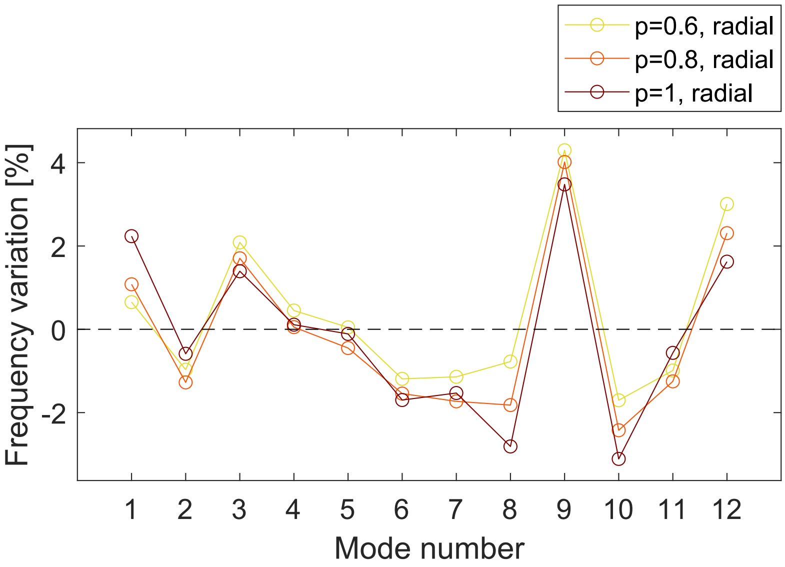

Figure 3.16: Percentage variation of the eigenfrequencies for the braced plates in simply supported boundary conditions, with different hole sizes and orientations, with respect to the eigenfrequencies of the solid plate.

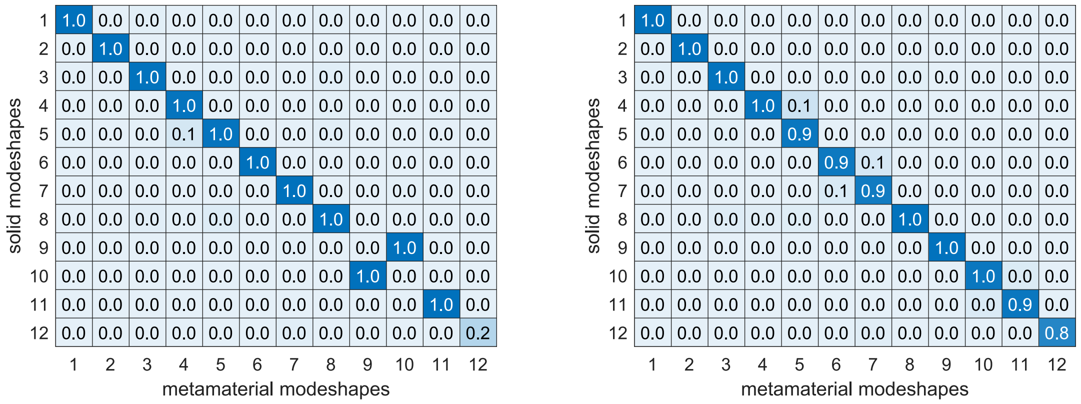

	1	2	3	4	5	6	7	8	9	10	11	12
1	1.0	0.0	0.0	0.0	0.0	0.0	0.0	0.0	0.0	0.0	0.0	0.0
2	0.0	1.0	0.0	0.0	0.0	0.0	0.0	0.0	0.0	0.0	0.0	0.0
3	0.0	0.0	1.0	0.0	0.0	0.0	0.0	0.0	0.0	0.0	0.0	0.0
4	0.0	0.0	0.0	1.0	0.0	0.0	0.0	0.0	0.0	0.0	0.0	0.0
5	0.0	0.0	0.0	0.1	1.0	0.0	0.0	0.0	0.0	0.0	0.0	0.0
6	0.0	0.0	0.0	0.0	0.0	1.0	0.0	0.0	0.0	0.0	0.0	0.0
7	0.0	0.0	0.0	0.0	0.0	0.0	1.0	0.0	0.0	0.0	0.0	0.0
8	0.0	0.0	0.0	0.0	0.0	0.0	0.0	1.0	0.0	0.0	0.0	0.0
9	0.0	0.0	0.0	0.0	0.0	0.0	0.0	0.0	0.0	1.0	0.0	0.0
10	0.0	0.0	0.0	0.0	0.0	0.0	0.0	0.0	1.0	0.0	0.0	0.0
11	0.0	0.0	0.0	0.0	0.0	0.0	0.0	0.0	0.0	0.0	1.0	0.0
12	0.0	0.0	0.0	0.0	0.0	0.0	0.0	0.0	0.0	0.0	0.0	0.2

	1	2	3	4	5	6	7	8	9	10	11	12
1	1.0	0.0	0.0	0.0	0.0	0.0	0.0	0.0	0.0	0.0	0.0	0.0
2	0.0	1.0	0.0	0.0	0.0	0.0	0.0	0.0	0.0	0.0	0.0	0.0
3	0.0	0.0	1.0	0.0	0.0	0.0	0.0	0.0	0.0	0.0	0.0	0.0
4	0.0	0.0	0.0	1.0	0.1	0.0	0.0	0.0	0.0	0.0	0.0	0.0
5	0.0	0.0	0.0	0.0	0.9	0.0	0.0	0.0	0.0	0.0	0.0	0.0
6	0.0	0.0	0.0	0.0	0.0	0.9	0.1	0.0	0.0	0.0	0.0	0.0
7	0.0	0.0	0.0	0.0	0.0	0.1	0.9	0.0	0.0	0.0	0.0	0.0
8	0.0	0.0	0.0	0.0	0.0	0.0	0.0	1.0	0.0	0.0	0.0	0.0
9	0.0	0.0	0.0	0.0	0.0	0.0	0.0	0.0	1.0	0.0	0.0	0.0
10	0.0	0.0	0.0	0.0	0.0	0.0	0.0	0.0	0.0	1.0	0.0	0.0
11	0.0	0.0	0.0	0.0	0.0	0.0	0.0	0.0	0.0	0.0	0.9	0.0
12	0.0	0.0	0.0	0.0	0.0	0.0	0.0	0.0	0.0	0.0	0.0	0.8

Figure 3.17: MAC matrices comparing the modal shapes of the braced metamaterial soundboards in simply supported boundary conditions with those of the solid soundboard. On the left the matrix referring to the case with the longitudinal holes (p=1), on the right the matrix referring to the case with the radial holes (p=1).

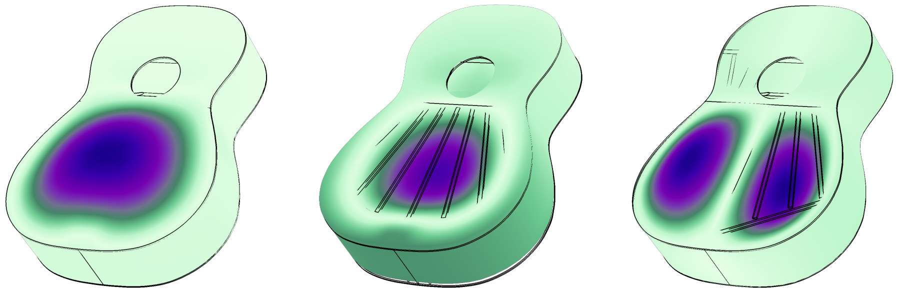

Figure 3.18: Mode shapes for the first 3 eigenfrequencies of the complete guitar body with a solid top.

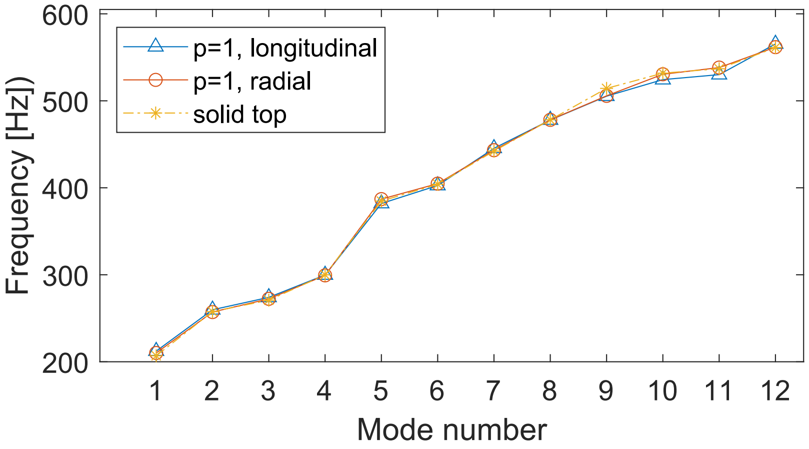

Figure 3.19: First 12 eigenfrequencies for the complete body of the guitar, in three cases: with longitudinal holes (p=1), with radial holes (p=1) and with the solid top.

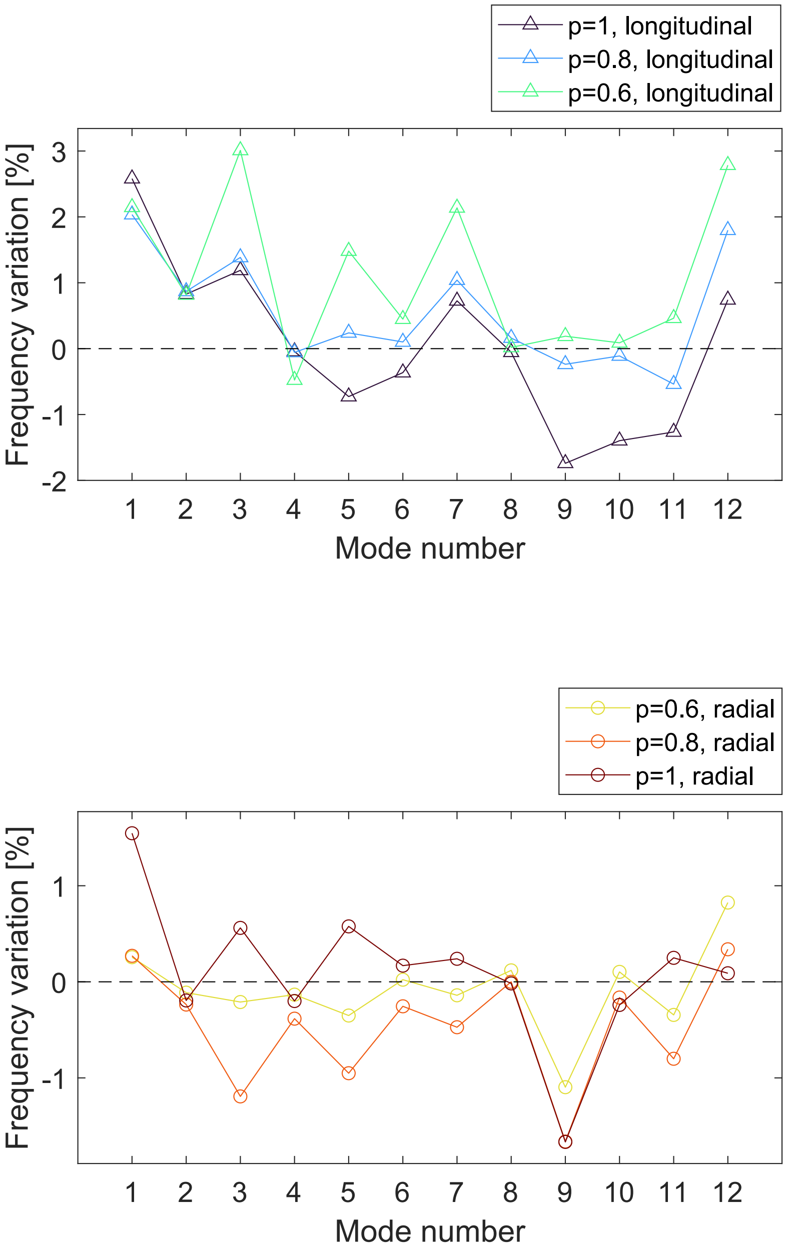

Figure 3.20: Percentage variation of the eigenfrequencies for the complete body of the guitar, with different hole sizes and orientations, with respect to the eigenfrequencies of the body with the solid plate.

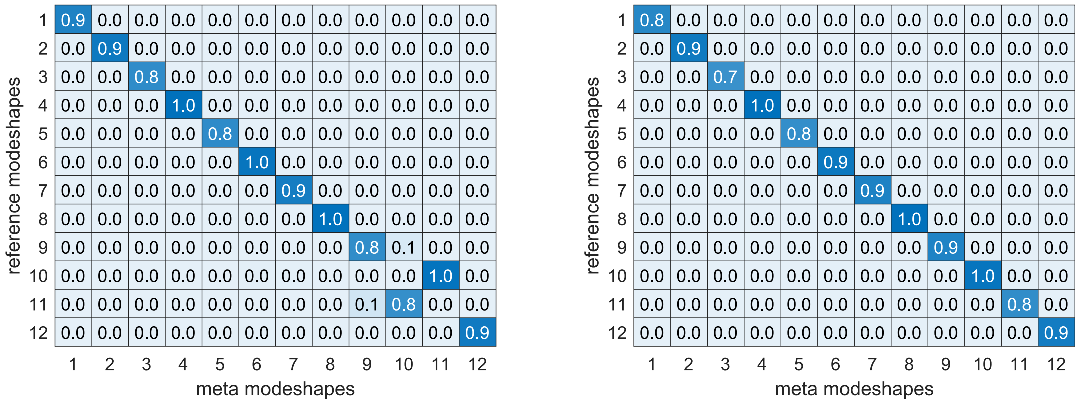

	1	2	3	4	5	6	7	8	9	10	11	12
1	0.9	0.0	0.0	0.0	0.0	0.0	0.0	0.0	0.0	0.0	0.0	0.0
2	0.0	0.9	0.0	0.0	0.0	0.0	0.0	0.0	0.0	0.0	0.0	0.0
3	0.0	0.0	0.8	0.0	0.0	0.0	0.0	0.0	0.0	0.0	0.0	0.0
4	0.0	0.0	0.0	1.0	0.0	0.0	0.0	0.0	0.0	0.0	0.0	0.0
5	0.0	0.0	0.0	0.0	0.8	0.0	0.0	0.0	0.0	0.0	0.0	0.0
6	0.0	0.0	0.0	0.0	0.0	1.0	0.0	0.0	0.0	0.0	0.0	0.0
7	0.0	0.0	0.0	0.0	0.0	0.0	0.9	0.0	0.0	0.0	0.0	0.0
8	0.0	0.0	0.0	0.0	0.0	0.0	0.0	1.0	0.0	0.0	0.0	0.0
9	0.0	0.0	0.0	0.0	0.0	0.0	0.0	0.0	0.8	0.1	0.0	0.0
10	0.0	0.0	0.0	0.0	0.0	0.0	0.0	0.0	0.0	0.0	1.0	0.0
11	0.0	0.0	0.0	0.0	0.0	0.0	0.0	0.0	0.1	0.8	0.0	0.0
12	0.0	0.0	0.0	0.0	0.0	0.0	0.0	0.0	0.0	0.0	0.0	0.9

	1	2	3	4	5	6	7	8	9	10	11	12
1	0.8	0.0	0.0	0.0	0.0	0.0	0.0	0.0	0.0	0.0	0.0	0.0
2	0.0	0.9	0.0	0.0	0.0	0.0	0.0	0.0	0.0	0.0	0.0	0.0
3	0.0	0.0	0.7	0.0	0.0	0.0	0.0	0.0	0.0	0.0	0.0	0.0
4	0.0	0.0	0.0	1.0	0.0	0.0	0.0	0.0	0.0	0.0	0.0	0.0
5	0.0	0.0	0.0	0.0	0.8	0.0	0.0	0.0	0.0	0.0	0.0	0.0
6	0.0	0.0	0.0	0.0	0.0	0.9	0.0	0.0	0.0	0.0	0.0	0.0
7	0.0	0.0	0.0	0.0	0.0	0.0	0.9	0.0	0.0	0.0	0.0	0.0
8	0.0	0.0	0.0	0.0	0.0	0.0	0.0	1.0	0.0	0.0	0.0	0.0
9	0.0	0.0	0.0	0.0	0.0	0.0	0.0	0.0	0.9	0.0	0.0	0.0
10	0.0	0.0	0.0	0.0	0.0	0.0	0.0	0.0	0.0	1.0	0.0	0.0
11	0.0	0.0	0.0	0.0	0.0	0.0	0.0	0.0	0.0	0.0	0.8	0.0
12	0.0	0.0	0.0	0.0	0.0	0.0	0.0	0.0	0.0	0.0	0.0	0.9

Figure 3.21: MAC matrices comparing the modal shapes of the body with the metamaterials with those of the solid one. On the left the matrix for the case of the longitudinal holes (p=1), on the right the one for the case of the radial holes (p=1).

3.3. Deformation under static load

Next, simulations of the deformation of the soundboard under a static load were performed. The goal of these simulations is to assess the amount of warping in the soundboard caused by the tension of the strings. This effect could indeed be accentuated to an excessive degree in a metamaterial instrument, so we seek to quantify it in the numerical model we have built. The results will also allow us to compare the bending stiffness of the different soundboards with realistic boundary conditions and loads.

The static load simulations have been performed on the complete model of the guitar body, including the bridge. A fixed constraint is imposed on the outer surface of the ribs, while the load is applied on the lower side of the bridge as shown in Fig. 3.22. Assuming a typical range of tensions of 50-80 N for nylon guitar strings [43], we used a total force of 480 N; this load is uniformly distributed on six small circular areas with a radius of 1 mm, corresponding with the points where the strings would be mounted in a real guitar.

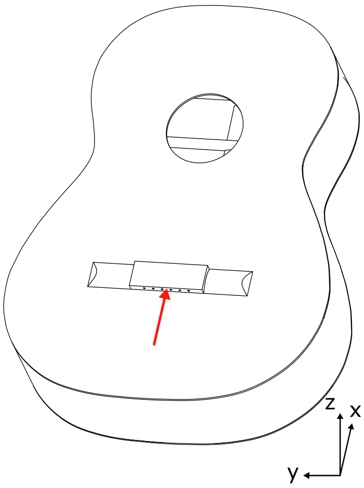

Figure 3.22: 3D model of the guitar body with the bridge. The red arrow shows the direction of the applied load.

3.3.1. Effect of varying hole size and orientation

First, we computed the displacement field of the top plate for various hole sizes in both longitudinal and radial orientation. Fig. 3.23 shows the normal displacement on the surface of the soundboards for some of the longitudinal holes. As expected, the warping appears to be accentuated when increasing the size of the holes.

In order to quantify the variation in stiffness compared to the variation in mass of the different soundboards, a scalar value quantifying the average magnitude of the deformation

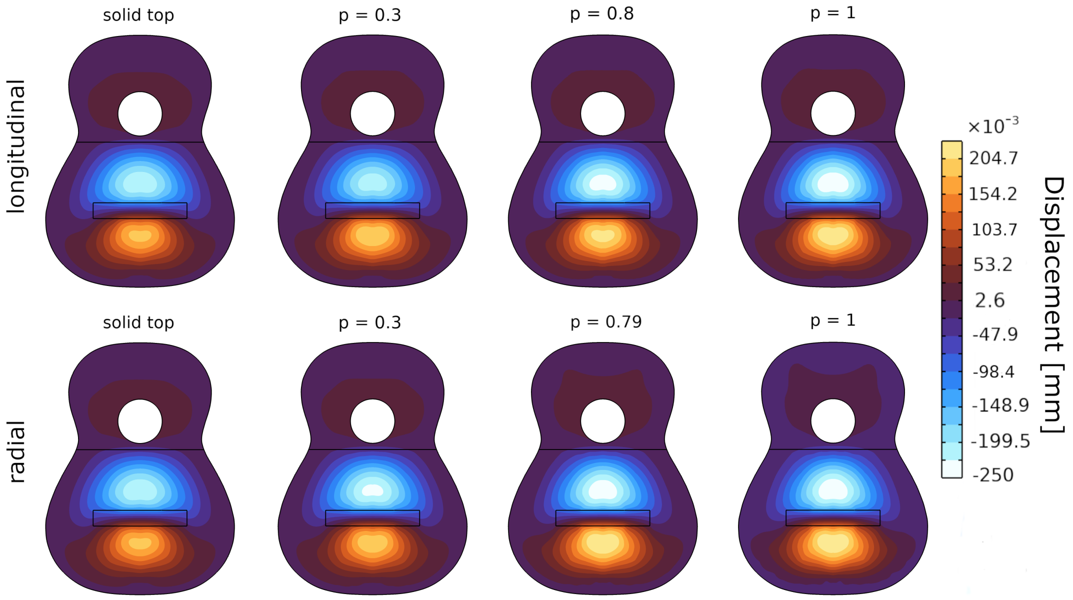

Figure 3.23: Normal displacement on the surface of the soundboard under the static load for different sizes of the holes. The top row shows results for the longitudinal holes, while the bottom row shows results for the radial holes.

is needed. For this purpose, the quadratic mean of the normal displacement w over the top surface was used, in the form:

$$w_{RMS} = \sqrt{\frac{1}{A}\int_A |w|^2 dxdy} \tag{3.1}$$

where A refers to the surface of the soundboard. Fig. 3.24(a) shows the values obtained from the simulations, as a function of the effective density of the lower bout ρ_{eff}. It's clear how the deformation increases for lower densities (larger holes) both for the longitudinal and radial orientations. However, as we discussed in Chapter 1, the decrease in stiffness must be compared to the decrease in mass, as our main goal is to obtain a soundboard that is both very light and relatively stiff. As such, we seek to increase the sound radiation coefficient $R = \sqrt{E/\rho^3}$, already introduced in Section 1.2. At this point we need to introduce an assumption in order to give an estimate of this quantity: we will assume that, given that the load case is identical, the RMS value of the displacement is inversely proportional to the effective longitudinal modulus of elasticity of the material. We can then observe the relative change in the R coefficient by computing the quantity $\sqrt{1/(\rho_{eff}^3 w_{RMS})}$. The black dotted lines in Fig. 3.24 are the constant-value curves of this quantity: clearly there is an increment for diminishing density. This is even more evident in Fig. 3.25, where the values of the same quantity normalized to the value for the solid top are displayed as a function of the effective density: the relative change reaches +27% for the largest longitudinal holes.

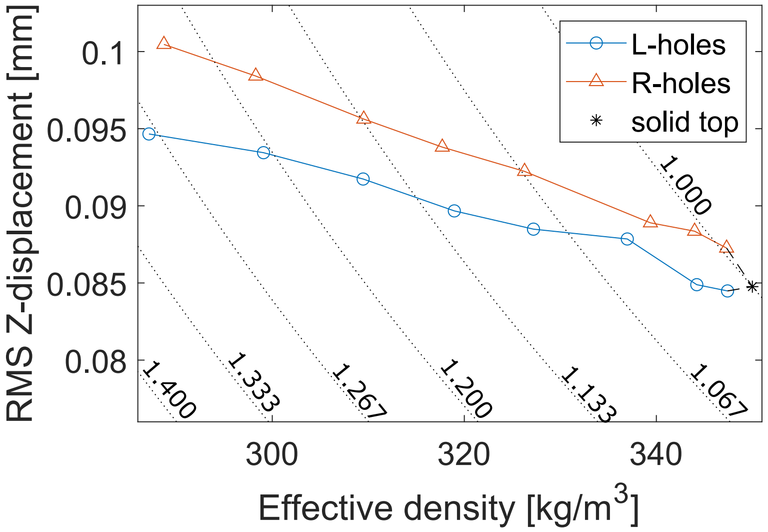

Figure 3.24: RMS value of the normal displacement on the surface of the soundboards, as a function of the effective density in the lower bout ρ_{eff}. The black dotted lines are constant-value curves of $\sqrt{1/(\rho_{eff}^3 w_{RMS})}$. The values they refer to are reported normalized by the value for the the solid top.

In order to further asses the capacity of the metamaterial instruments to withstand the tension of the strings, we can also look at the distribution of stresses in the soundboard. Unfortunately, we cannot develop a way to predict failure, as failure theories in anisotropic materials require the definition of a number of constants to be determined experimentally [44]. However, looking at the Von Mises stress can still give us an idea of where stresses are concentrated, as wall as provide us with a way to gauge the differences in the stress state between different configurations. Fig. 3.26 shows the Von Mises stress for the case of the solid plate and for a few metamaterial soundboards with different hole sizes and orientations. As expected, stresses throughout the plate are accentuated when increasing the holes size. The plates with radial holes, however, seem to exhibit a greater concentration of stresses around the area of the bridge, which points to an increased potential for failure of the material. This, together with our analysis of the deformation of the soundboard, suggest that the longitudinal holes are a more suitable design choice when it comes to the stability of the instrument under the tension of the strings.

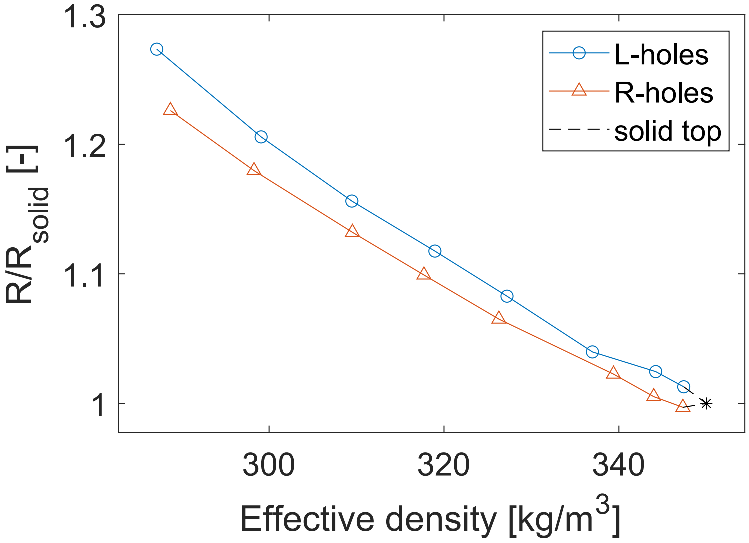

Figure 3.25: Values of $\sqrt{1/(\rho_{eff}^3 w_{RMS})}$ normalized to the value for the solid top (marked in the graph by a black asterisk).

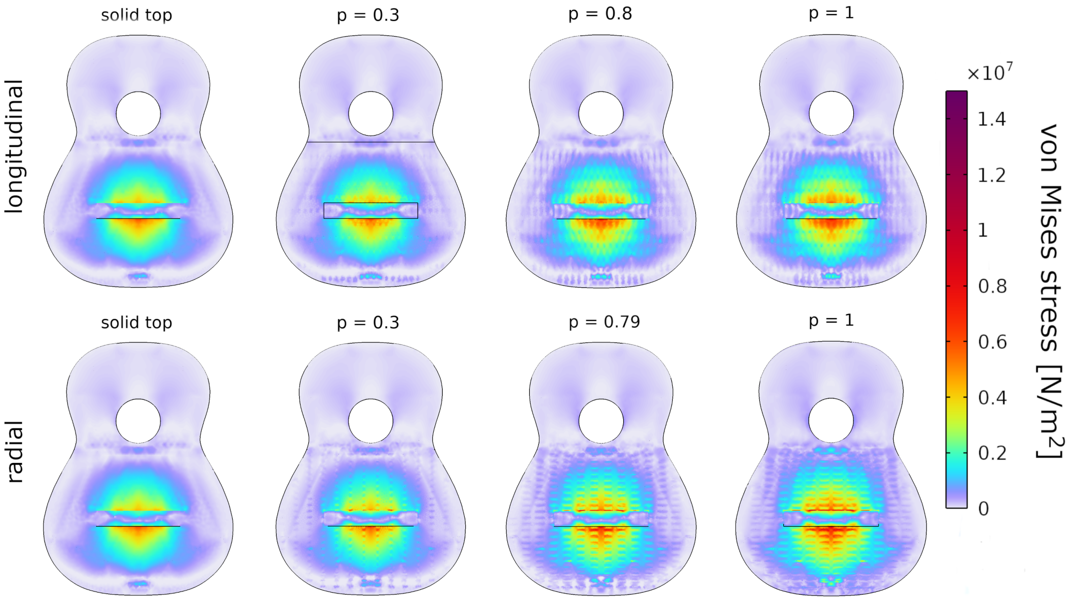
solid top
p = 0.3
p = 0.8
p = 1
longitudinal
solid top
p = 0.3
p = 0.79
p = 1
radial
×10^7
1.4
1.2
1
0.8
0.6
0.4
0.2
0
von Mises stress [N/m^2]

Figure 3.26: Von Mises stress on the surface of the soundboard under the static load for different sizes of the holes. The top row shows results for the longitudinal holes, while the bottom row shows results for the radial holes.

3.3.2. Compensating with the braces

Next, we turned our attention to trying to compensate for the loss of stiffness by adding thickness to the fan braces: the goal is to make up for the increased warping without re-adding too much mass to the structure. Here we focus exclusively on the case of longitudinal holes with $p = 1$. The braces are originally 3 mm thick, and they have been uniformly increased in thickness in 0.5 mm increments up to 5 mm total. These changes have not been applied at the same time to all seven fan braces, however: referencing Fig. 2.3 and numbering the braces from left to right, they have been applied first to the central brace (brace 4), and then to the three pairs of braces 1 and 7, 2 and 6, and 3 and 5. The simulations are set up in the exact same way as those in the previous section. We focus here exclusively on the largest longitudinal holes (p=1) as, by the metrics we estabilished earlier, that particular choice seemed to be the most promising one. There is, however, no particular reason to expect that the effects observed when varying the thickness of the braces would be qualitatively different with a different size or orientation of the holes.

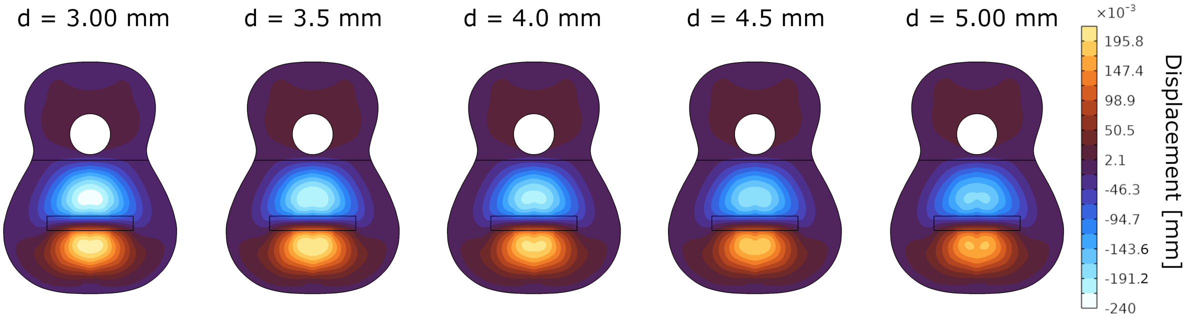

Figure 3.27: Normal displacement on the surface of the soundboard for varying thickness of the central brace (brace 4), indicated as d. The soundboard used here is the one with longitudinal holes, $p = 1$.

Fig. 3.27 shows the normal displacement on the surface of the soundboard for different values of the thickness of the central brace (brace 4), denoted as d. Comparison between the graphs seems to suggest that there is indeed a reduction in the deformation as d is increased, as is very much expected. However our stated goal here is to recover the same deformation observed in the case of the solid plate, so we need a way to compare how close to this case we get with any choice of brace thickness. This is done by defining a scalar quantity meant to evaluate the difference between the deflection shapes of the metamaterial surface and that of the solid plate. Such quantity is defined as the quadratic mean of the difference between the normal displacements:

$$\overline{w - w_{solid}} = \sqrt{\frac{1}{A}\int_A |w - w_{solid}|^2 dxdy} \tag{3.2}$$

where w is the normal displacement on the surface of the metamaterial plate and w_{solid} is the normal displacement on the surface of the solid plate.

Figure 3.28 shows the values of this quantity computed for different thicknesses of the braces. It's immediately apparent that varying the outermost pairs of braces, i. e. the pairs (1,7) and (2,6), has little if any effect on the deflection shape of the board. This is expected, as most of the deformation is localized in the middle of the lower bout, around the bridge. When it comes to the pair (3,5), adding thickness has a clear effect on the RMS difference: we see that by adding up to 1 mm of material there's a reduction, while going further results in an "overcorrection" of sorts. Finally, for the central brace, increasing the thickness further, up to 4.5 mm, seems to have the best compensating effect overall. Having observed this behavior, a quadratic fit to the data has been performed, as reported in Fig. 3.28. The resulting parabolic functions have minima at $d = 4.13$ mm for braces 3 and 5, and at $d = 4.78$ mm for brace 4. However, the reduction in the RMS difference for brace 4 at thickness $d = 4.5$ mm can be considered already satisfactory, and it comes at the small cost of adding back 0.88 g of material to the soundboard.

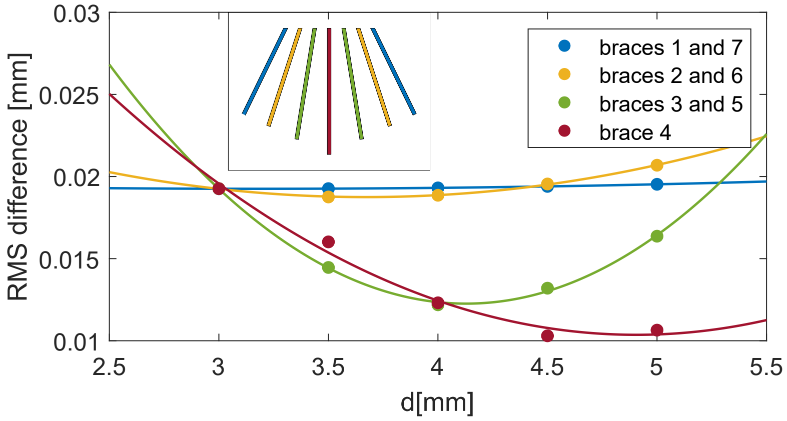

Figure 3.28: Quadratic average over the lower bout of the difference between the displacements in the metamaterial soundboards and the solid plate, computed as in (3.2). The values are reported for varying thickness of the braces: these were altered in pairs, except for the central one. The solid lines represent the results of a best fit to a quadratic polynomial. A diagram of the 7 fan braces with the same color coding used in the plot is also shown.

3.4. Mobility at the bridge

Returning our focus onto the dynamic behavior of the instruments, frequency domain simulations were performed to evaluate the frequency response of the guitar body models. These were obtained by imposing a normal, harmonic load on a circular area with a 2 mm radius on the top surface of the soundboard, located under the bridge, in the middle of the lower bout. The normal component of the velocity was then recovered at the same place, in order to measure the driving-point mobility. The numerical model here differs from the one used in Sec. 3.2.5 in one way: whereas earlier we ignored the effect of structural damping, here it is accounted for in the form of proportional, or Rayleigh damping. In particular, following [45], we use a stiffness-proportional damping matrix, in the following form:

$$C = \beta K \tag{3.3}$$

where C and K are the damping and stiffness matrices of the finite element model, and $\beta = 2 \cdot 10^{-6}$ s. No mass-proportional damping term is included in order to avoid over-damping at low frequencies.
Fig. 3.29 shows the magnitudes of the driving-point mobility for the solid top and for the top plates with the largest holes in both the longitudinal and radial orientations. In order to compare the mobilities at resonance, simulations were also ran at the eigenfrequencies corresponding to the first three peaks in Fig. 3.29. This gives us the possibility of directly comparing the peak magnitudes of the mobility in the different cases. The results can be seen in Fig. 3.30 and 3.31, which show the peak mobilities with longitudinal and radial holes respectively, reported as a function of the effective density. Overall, we observe an upwards trend with decreasing density (increasing hole size), but the effect is not particularly pronounced.

Another way to compare the different mobility response functions is to compute the average of their magnitude. After all, as explained in Chapter 1, the main effect of raising the sound radiation coefficient R should be an increase of the mean value of the mobility. Fig. 3.32 shows the average values of the mobility for different cases, with both longitudinal and radial holes, as a function of the effective density. Here we can see a stronger effect of the metamaterials, with a clear increase in the average level compared to the solid top for all the cases under study. Furthermore, there seems to be an upwards trend with decreasing density, particularly for the longitudinal holes. This effect, however, is not very clear-cut: for instance, the largest observed value, the one for longitudinal holes with $\rho_{eff} = 299.09\,\mathrm{kg\,m^{-2}}$ (p=0.9), is indeed larger than the value for longitudinal holes at $\rho_{eff} = 287.15\,\mathrm{kg\,m^{-2}}$.

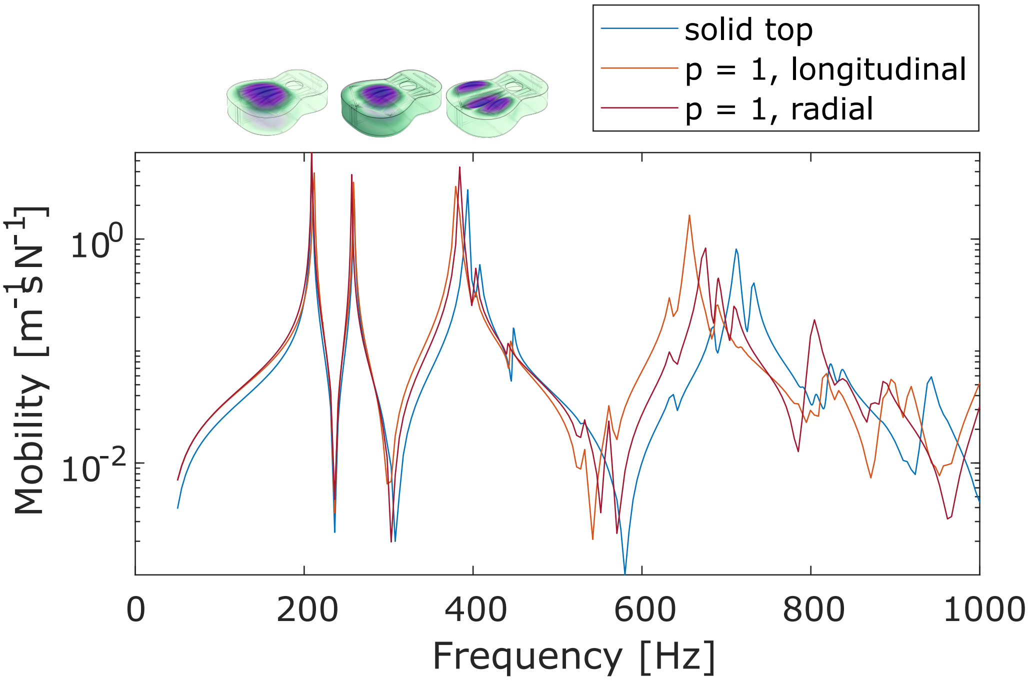

Figure 3.29: Magnitude of the driving-point mobility at the bridge location, for the solid top and two of the metamaterial plates. Above the the first three peaks the shapes of the first three modes are reported. The first mode involves ”breathing” motion of the structure, with the top and back plate moving outwards in phase; The relative phase between the two plates is instead inverted in the second mode.

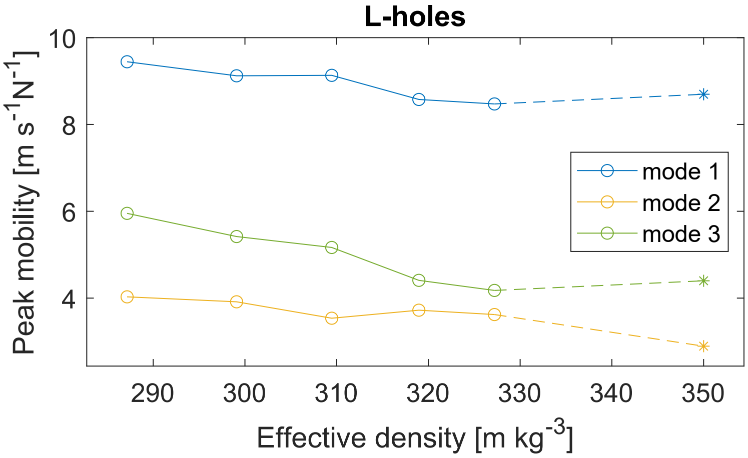

Figure 3.30: Magnitudes of the mobility at resonance for the first three peaks for the longitudinal holes, with varying hole size, reported as a function of the effective density. The asterisks correspond to the results for the body with the solid top.

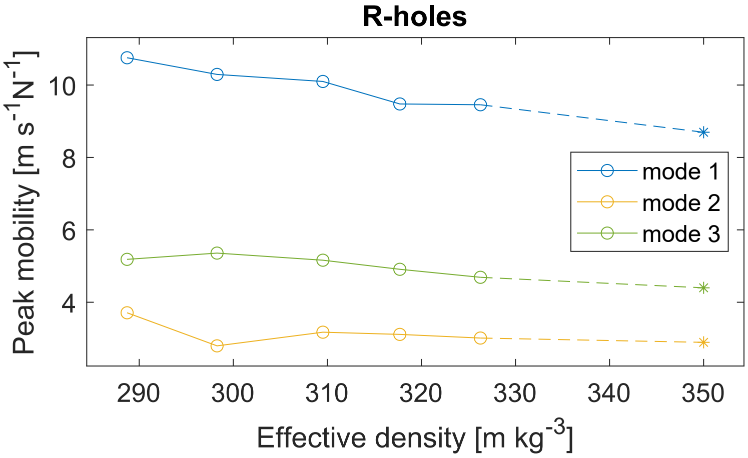

Figure 3.31: Magnitudes of the mobility at resonance for the first three peaks for the radial holes, with varying hole size, reported as a function of the effective density. The asterisks correspond to the results for the body with the solid top.

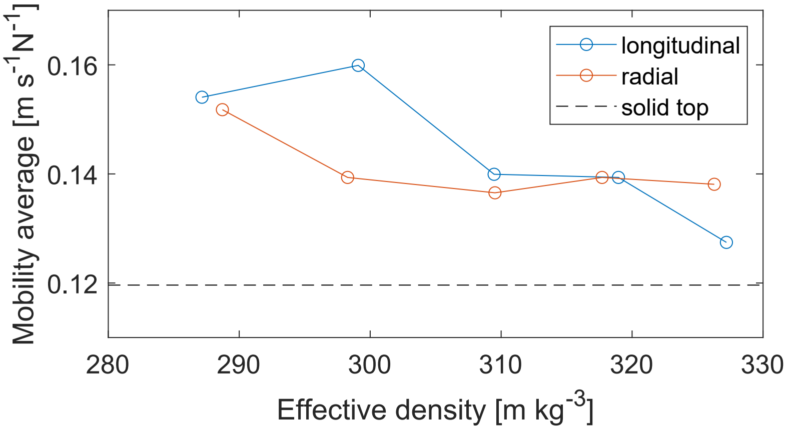

Figure 3.32: Average of the mobility for varying hole size, reported as a function of the effective density. Results for both longitudinal and radial holes are reported. The horizontal dotted line represents the average of the mobility for the body with the solid top plate.

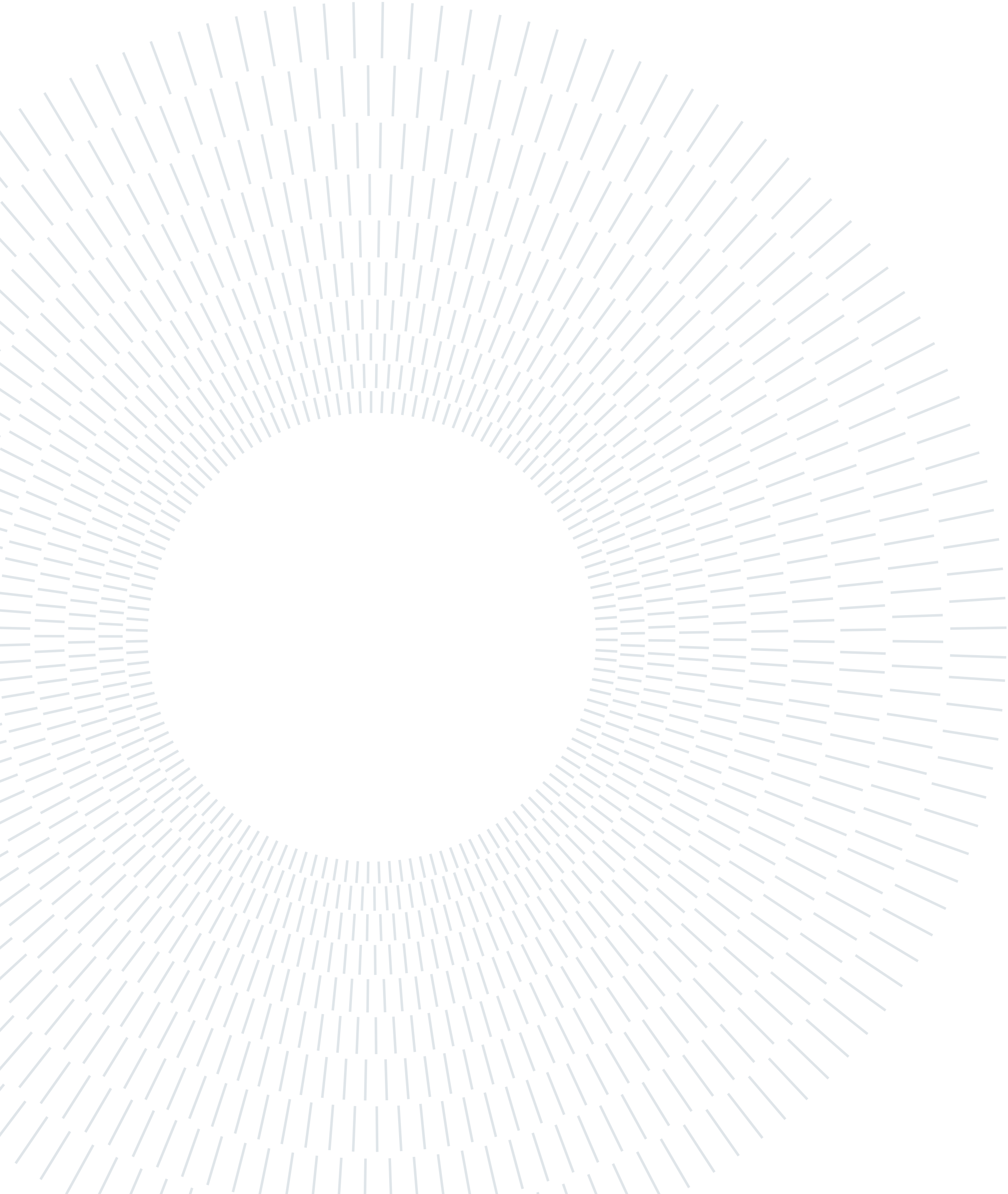

4 | Conclusions

The aim of the present work was to evaluate the effect of the use of wooden mechanical metamaterials in a classical guitar's soundboard, in order to establish if these materials could represent a useful tool for luthiers and manufacturers. We have accomplished this by way of numerical simulations, building a numerical model of the instrument where we could vary the orientation and size of the holes of the metamaterial in order to compare the effect of different geometries. The reference for the construction of this model is an instrument built by Antonio de Torres in 1864, which was then modified as needed by the introduction of the hole patterns that implement the metamaterial. The reference was chosen as the design of this and other similar instruments represents a hallmark in the tradition of guitar making. Using this design as our base point, then, allowed us to study the effect of an innovative material in an otherwise very traditional instrument.

Our studies have shown that the use of mechanical metamaterials in the soundboards of classical guitars is feasible, and under many aspects, beneficial. We have found that the introduction of the metamaterials does not modify radically the modal behavior of the instruments, meaning that the timbral characteristics of the guitar are preserved, and that the difference between the different orientations of the elliptical holes do not produce vastly different outcomes. We have thus shown that the variation in the mechanical properties of the plates found in [10] have a somewhat reduced impact on the mechanics of the complete instrument. This, however, is not surprising: we know from the literature that the vibrational behavior of a guitar is strongly influenced by many different material parameters corresponding to the various components of the instrument, and the elastic moduli of the soundboard are not the most important in this respect [46].

A stronger effect has been observed in the deformation of the soundboard under the static load imposed by the tension of the strings. With the simulations we performed we found that, as expected, the introduction of the metamaterials increases the extent of the warping that the soundboard undergoes when the strings are mounted and tuned. This effect is accentuated when increasing size of the holes. Most importantly, though, it appears to be more pronounced in the case of the radial holes, as with this choice of orientation the effective stiffness of the top plate in the longitudinal direction (parallel to the applied load) is smaller. This shows that the orientation of the holes is relevant at least for what concerns the load-bearing capacity of the instrument, and that in this respect the longitudinal holes are preferable to the radial holes. Soundboards with longitudinal holes were indeed also shown to be advantageous when comparing the increase in the deformation (sign of a decreased stiffness) to the corresponding reduction in mass. One of our goals is raising the effective sound radiation coefficient $R = \sqrt{E/\rho^3}$ of the soundboard, and the fact that we saw significantly less pronounced deformation in the soundboards with longitudinal holes compared to those with radial holes for similar effective densities means that we expect a better performance of the former in terms of sound radiation. We have also shown that the increased deformation can be corrected for by slightly increasing the thickness of one of the fan braces of the soundboard. Therefore, by adding back very little mass to the plate we can have a very light top plate which can still bear the load of the strings like a regular solid plate.

Finally, we have also studied the effects of the metamaterials on the admittance spectrum of the instrument. As we have seen in the modal analysis, the shape of the frequency response does not appear to be heavily impacted. However, an important effect was observed, which we expect to see when raising the sound radiation coefficient of the soundboard: the average level of the admittances is raised significantly. Effectively, this means that the metamaterial instruments are overall louder, a feature which is highly sought after in classical guitars. The average levels seem to be overall slightly higher with longitudinal holes than with radial holes, indicating that the former design might be preferable.

Our results are novel as very few works on the application of mechanical metamaterials to the construction of musical instruments can be found in the literature. These new materials could be a very useful tool for instrument makers, as they could afford them a new degree of control over the vibrational response of their instruments. They also have the potential to allow for the use of some kinds of woods that are not usually employed in fine instruments, or to let makers make a more efficient use of the existing supplies of the species of wood that are traditionally used. This is important as the supply of the woods typically used in instrument making are especially prone to shortages, a problem which is only going to worsen with increasing climate change. These findings, moreover, could prove to be of great interest even beyond the field of musical acoustics, as they could represent a starting point to study the applications of wooden metamaterials to all kinds of complex structures.

4.1. Future Works

In this work we have only studied the application of a few particular configurations of the hole patterns that make up the metamaterials to a particular instrument, the classical guitar. Our results could be expanded upon by performing the same studies with different configurations: this could mean changing different parameters of the elliptical holes, such as the aspect ratio and orientation, or exploring hole patterns with nonuniform hole sizes, or studying different shapes and tilings of the unit cells. Our work could also be complemented by the addition of a coupling of the structure with the acoustic field, which would allow for a more direct way to investigate the sound radiation properties of the instrument. Moreover, similar studies can also be conducted on other instruments which feature a wooden plate as one of the main radiating elements: this has already been done, for example, by fellow student Gabriele Marelli in his master's thesis [34] for the *cajón peruano*, but similar designs could be applied to a number of stringed and percussion instruments.

However, the future development that our numerical studies calls for the most is, naturally, experimental validation. This means building real instruments based on our virtual designs, and performing experiments to quantitatively characterize their mechanical and acoustical properties, as well as evaluating subjectively their sound and timbre. Building real world prototypes would allow for a definitive assessment of the feasibility and of the (expected) advantages of metamaterial instruments. The realization of the metamaterial soundboards can be faithfully reproduced from our CAD designs with the use of a CNC machine, allowing for direct validation of the numerical models. Planning for the realization of this next phase in the study of metamaterials for instrument making has been under way for a few months at time of writing, and experiments will be carried out by collaborators at Politecnico di Milano and Universidad de Chile.

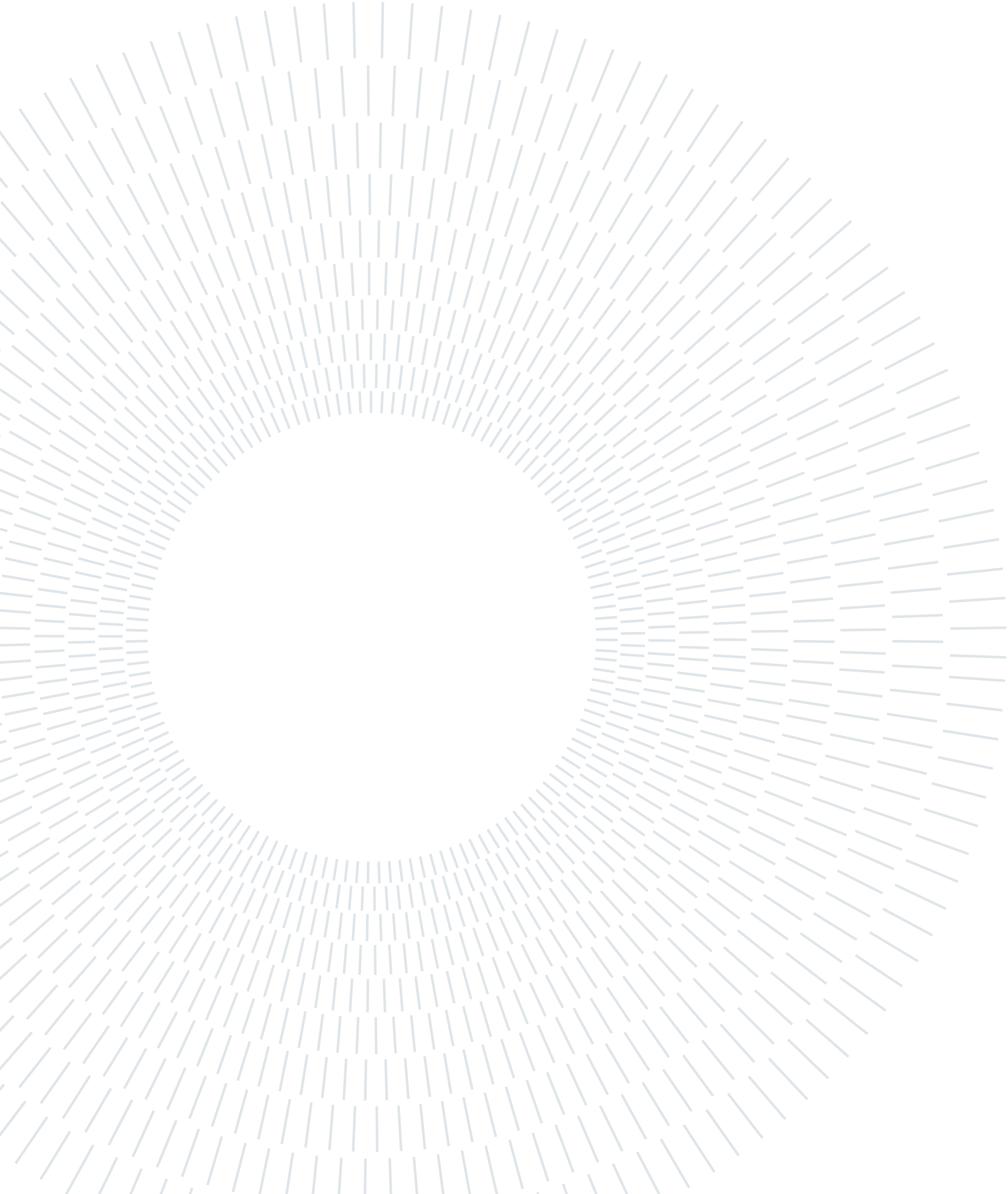

Bibliography

[1] C. Barlow, “Materials selection for musical instruments,” *Proceedings institute of acoustics*, vol. 19, pp. 69–78, 1997.

[2] U. G. Wegst, “Wood for sound,” *American Journal of Botany*, vol. 93, no. 10, pp. 1439–1448, 2006.

[3] C. Gibson and A. Warren, “Resource-sensitive global production networks: reconfigured geographies of timber and acoustic guitar manufacturing,” *Economic Geography*, vol. 92, no. 4, pp. 430–454, 2016.

[4] J. Lenoir, J.-C. Gégout, P. Marquet, P. De Ruffray, and H. Brisse, “A significant upward shift in plant species optimum elevation during the 20th century,” *science*, vol. 320, no. 5884, pp. 1768–1771, 2008.

[5] C. J. Maxwell and R. M. Scheller, “Identifying habitat holdouts for high elevation tree species under climate change,” *Frontiers in Forests and Global Change*, p. 94, 2020.

[6] T. Gore, “Wood for guitars,” in *Proceedings of Meetings on Acoustics 161ASA*, vol. 12, p. 035001, Acoustical Society of America, 2011.

[7] R. Viala, V. Placet, and S. Cogan, “Simultaneous non-destructive identification of multiple elastic and damping properties of spruce tonewood to improve grading,” *Journal of Cultural Heritage*, vol. 42, pp. 108–116, 2020.

[8] E. Nader Engheta, Richard W. Ziolkowski, *Electromagnetic Metamaterials: Physics and Engineering Explorations*. Wiley-IEEE Press, 1 ed., 2006.

[9] X. Yu, J. Zhou, H. Liang, Z. Jiang, and L. Wu, “Mechanical metamaterials associated with stiffness, rigidity and compressibility: A brief review,” *Progress in Materials Science*, vol. 94, pp. 114–173, 2018.

[10] S. Gonzalez, E. Chacra, C. Carreño, and C. Espinoza, “Wooden mechanical metamaterials: from guitar-making to tunable wood,” *submitted to Materials and Design*, 2022.

[11] J. Lemaitre and J.-L. Chaboche, *Mechanics of Solid Materials.* Cambridge University Press, 1990.

[12] O. M. S. Arthur P. Boresi, Richard J. Schmidt, *Advanced mechanics of materials.* Wiley, 5th ed ed., 1993.

[13] R. J. Ross, *Wood Handbook.* USDA, FPL-GTR-190, 2010.

[14] A. Chaigne and J. Kergomard, *Acoustics of Musical Instruments.* New York: Springer-Verlag, 2016.

[15] M. Quintavalla, F. Gabrielli, and C. Canevari, "Grading materials for stringed instruments soundboards: An approach considering the orthotropic elastic and damping properties," *Applied Acoustics*, vol. 187, p. 108521, 2022.

[16] E. Skudrzyk, "The mean-value method of predicting the dynamic response of complex vibrators," *The Journal of the Acoustical Society of America*, vol. 67, no. 4, pp. 1105–1135, 1980.

[17] J. B. Pendry, "Negative refraction makes a perfect lens," *Physical review letters*, vol. 85, no. 18, p. 3966, 2000.

[18] R. A. Shelby, D. R. Smith, and S. Schultz, "Experimental verification of a negative index of refraction," *science*, vol. 292, no. 5514, pp. 77–79, 2001.

[19] M. Maldovan, "Sound and heat revolutions in phononics," *Nature*, vol. 503, no. 7475, pp. 209–217, 2013.

[20] M. Wegener, "Metamaterials beyond optics," *Science*, vol. 342, no. 6161, pp. 939–940, 2013.

[21] K. Bertoldi, P. M. Reis, S. Willshaw, and T. Mullin, "Negative poisson's ratio behavior induced by an elastic instability," *Advanced Materials*, vol. 22, no. 3, pp. 361–366, 2010.

[22] R. Lakes, "Foam structures with a negative poisson's ratio," *Science*, vol. 235, no. 4792, pp. 1038–1040, 1987.

[23] T. Bückmann, M. Thiel, M. Kadic, R. Schittny, and M. Wegener, "An elastomechanical unfeelability cloak made of pentamode metamaterials," *Nature communications*, vol. 5, no. 1, pp. 1–6, 2014.

[24] R. S. Lakes, T. Lee, A. Bersie, and Y.-C. Wang, "Extreme damping in composite materials with negative-stiffness inclusions," *Nature*, vol. 410, no. 6828, pp. 565–567, 2001.

[25] Z. G. Nicolaou and A. E. Motter, “Mechanical metamaterials with negative compressibility transitions,” *Nature materials*, vol. 11, no. 7, pp. 608–613, 2012.

[26] X. Zheng, H. Lee, T. H. Weisgraber, M. Shusteff, J. DeOtte, E. B. Duoss, J. D. Kuntz, M. M. Biener, Q. Ge, J. A. Jackson, *et al.*, “Ultralight, ultrastiff mechanical metamaterials,” *Science*, vol. 344, no. 6190, pp. 1373–1377, 2014.

[27] R. Bader, J. Fischer, M. Münster, and P. Kontopidis, “Metamaterials in musical acoustics: A modified frame drum,” *The Journal of the Acoustical Society of America*, vol. 145, no. 5, pp. 3086–3094, 2019.

[28] L. Music.

[29] Rainsong.

[30] Blackbird.

[31] R. Viala, C. Fritz, V. Placet, E. Foltete, and S. Cogan, “Optimization of composites guitar plates recipes using non-destructive mechanical characterization in the dynamical domain,” in *Forum Acusticum*, pp. 3331–3331, 2020.

[32] E. Özdemir, L. Kiesewetter, K. Antorveza, T. Cheng, S. Leder, D. Wood, and A. Menges, “Towards self-shaping metamaterial shells,” in *The International Conference on Computational Design and Robotic Fabrication*, pp. 275–285, Springer, Singapore, 2021.

[33] G. Iannace, G. Ciaburro, and A. Trematerra, “Metamaterials acoustic barrier,” *Applied Acoustics*, vol. 181, p. 108172, 2021.

[34] G. Marelli, “Metamaterials in instruments making: cajon peruano case study,” Master’s thesis, Politecnico di Milano, Milan, 2022.

[35] R. Courtnall, *Making Master Guitars.* Hale/Stewart-MacDonald, 1993.

[36] J. L. Romanillos, *Antonio de Torres: Guitar Maker - His Life and Work.* Bold Strummer, 1997.

[37] I. Sloane, *Classic Guitar Construction.* Omnibus Press, 1976.

[38] “Comsol multiphysics ® v. 6.0.” `www.comsol.com`. COMSOL, Inc.

[39] A. Brauchler, P. Ziegler, and P. Eberhard, “An entirely reverse-engineered finite element model of a classical guitar in comparison with experimental data,” *The Journal of the Acoustical Society of America*, vol. 149, no. 6, pp. 4450–4462, 2021.

[40] "Structural mechanics module v. 5.6." `https://doc.comsol.com/5.6/doc/com.comsol.help.sme/StructuralMechanicsModuleUsersGuide.pdf`. COMSOL AB, Stockholm, Sweden.

[41] G. Caldersmith and E. Freeman, "Wood properties from sample plate measurements i," *J Catgut Acoust Soc*, vol. 1, no. series II, pp. 8–12, 1990.

[42] R. J. Allemang, "The modal assurance criterion–twenty years of use and abuse," *Sound and vibration*, vol. 37, no. 8, pp. 14–23, 2003.

[43] N. H. Fletcher and T. D. Rossing, *The Physics of Musical Instruments.* Springer, 1998.

[44] B. Kasal and R. J. Leichti, "State of the art in multiaxial phenomenological failure criteria for wood members," *Progress in Structural Engineering and Materials*, vol. 7, no. 1, pp. 3–13, 2005.

[45] J. A. Torres, C. A. Soto, and D. Torres-Torres, "Exploring design variations of the titian stradivari violin using a finite element model," *The Journal of the Acoustical Society of America*, vol. 148, no. 3, pp. 1496–1506, 2020.

[46] A. Brauchler, D. Hose, P. Ziegler, M. Hanss, and P. Eberhard, "Distinguishing geometrically identical instruments: Possibilistic identification of material parameters in a parametrically model order reduced finite element model of a classical guitar," *Journal of Sound and Vibration*, vol. 535, p. 117071, 2022.

List of Figures

1.1 The three principal axes of wood, from [13]. The picture shows the direction of the fibers, which coincides with the longitudinal axis, and the growth rings, which are perpendicular to the radial axis. 8

1.2 Comparison of a *quarter sawn* (left) and a *plain sawn* board, showing the reference frame of the principal axes of the wooden log. Image from [15]. . 10

1.3 (a) Octet-truss unit cells packed into a cubic microlattice [26]. This material exhibits vary high stiffness-to-density ratio. (b) 2D periodic porous structure, from [21]. The mechanical properties of this structure can be controlled by compressing it. 12

1.4 Example diagram of a wooden plate carved with a pattern of elliptical holes, from [10]. The image shows a periodic pattern obtained by the repeated juxtaposition of a unit cell. The authors varied the holes' size, aspect ratio and orientation to investigate the effect of these changes in the geometry on the elastic behavior of the plates. 13

1.5 Variation of the longitudinal and radial Young's moduli of the plates when varying the aspect ratio of the holes, for different effective densities, from [10]. The terms “longitudinal" and “radial", here as well as in later chapters, refer to the orientations of the holes' major axes with respect to the principal axes of the wood, as shown in the diagram reported alongside the graph. For the longitudinal modulus, the introduction of the holes results in a lowering of the value. The effect is compensated when the major axis of the ellipses is parallel to the longitudinal axis of the plate's wood, and it is accentuated when it's parallel to the radial axis. For the radial modulus, we see an analogous effect. 15

2.1 Exploded view of a classical guitar, from [37]. 19

2.2 Soundboard drawing used as a reference, from [35]. This is in turn modeled after a Torres guitar from 1864. All the dimensions in the figure are in mm. 20

2.3 Bottom view of the soundboard model with the bracing. 20

2.4 Model of the back plate, showing the three transverse braces, and the reinforcing strip. 21
2.5 Model of the ribs and blocks, assembled over the back plate. 22
2.6 Model of the bridge. 22
2.7 Diagram showing the underside of the solid top plate, as well as those with longitudinal (left) and radial (right) holes. The arrows show the directions of the longitudinal (L) and radial (R) axes of the plate's wood. The colors mark the height of each surface with respect to the lower surface of the plate. 23
2.8 Unit cells with three different hole sizes. The hole size is varied with a scaling parameter $p \leq 1$, while both the aspect ratio of the holes and the size of the cell are kept constant. 24
2.9 3D cut view of the model of the instrument's body, showing all the individual components and the material that was chose for the main parts. . . 24

3.1 Diagram of the workflow for the eigenfrequency simulations. The results in [10] have been obtained by studying the modal behavior of free rectangular plate. To investigate possible applications to guitar soundboards, we performed eigenfrequency studies on the soundboard by incrementally adding elements, increasing the complexity of the structure from the free unbraced plate toup to the complete body of the instrument. 28
3.2 Mode shapes of the unbraced solid soundboard in free boundary conditions for the 5 lowest eigenfrequencies, in ascending order from left to right. . . . 29
3.3 First 12 eigenfrequencies for the free, unbraced soundboard, with longitudinal holes (p=1), radial holes (p=1) and in the case of the solid plate. . . 30
3.4 Percentage variation of the eigenfrequencies for the unbraced plates in free boundary conditions, with different hole sizes and orientations, with respect to the eigenfrequencies of the solid plate. 31
3.5 Matrices of the MAC coefficients between the modal shapes of the free, unbraced metamaterial soundboards, and the modal shapes of the solid plate. On the left the matrix for the case of the longitudinal holes (p=1), on the right the one for the case of the radial holes (p=1). 32
3.6 Mode shapes of the unbraced solid soundboard in simply supported boundary conditions for the 5 lowest eigenfrequencies. 32
3.7 First 12 eigenfrequencies for the unbraced soundboard in simply supported boundary conditions, with longitudinal holes (p=1), radial holes (p=1) and in the case of the solid plate. 33

3.8 Percentage variation of the eigenfrequencies for the unbraced plates in simply supported boundary conditions, with different hole sizes and orientations, with respect to the eigenfrequencies of the solid plate. 34
3.9 Matrices of the MAC coefficients between the modal shapes of the unbraced metamaterial soundboards in simply supported boundary conditions, and the modal shapes of the solid plate. On the left the matrix for the case of the longitudinal holes (p=1), on the right the one for the case of the radial holes (p=1). 35
3.10 Mode shapes of the braced solid soundboard in free boundary conditions for the 5 lowest eigenfrequencies, in ascending order from left to right. . . . 35
3.11 First 12 eigenfrequencies for the braced soundboard in free boundary conditions, in three cases: with longitudinal holes (p=1), with radial holes (p=1) and the solid plate. 36
3.12 Percentage variation of the eigenfrequencies for the braced plates in free boundary conditions, with different hole sizes and orientations, with respect to the eigenfrequencies of the solid plate, in ascending order from left to right. 37
3.13 MAC matrices comparing the modal shapes of the free, braced metamaterial soundboards with those of the solid one. On the left the matrix for the case of the longitudinal holes (p=1), on the right the one for the case of the radial holes (p=1). 38
3.14 Mode shapes of the braced solid soundboard in simply supported boundary conditions for the 5 lowest eigenfrequencies. 39
3.15 First 12 eigenfrequencies for the braced soundboard in simply supported boundary conditions, in three cases: with longitudinal holes (p=1), with radial holes (p=1), and with the solid top. 40
3.16 Percentage variation of the eigenfrequencies for the braced plates in simply supported boundary conditions, with different hole sizes and orientations, with respect to the eigenfrequencies of the solid plate. 41
3.17 MAC matrices comparing the modal shapes of the braced metamaterial soundboards in simply supported boundary conditions with those of the solid soundboard. On the left the matrix referring to the case with the longitudinal holes (p=1), on the right the matrix referring to the case with the radial holes (p=1). 42
3.18 Mode shapes for the first 3 eigenfrequencies of the complete guitar body with a solid top. 42

3.19 First 12 eigenfrequencies for the complete body of the guitar, in three cases: with longitudinal holes (p=1), with radial holes (p=1) and with the solid top. 43

3.20 Percentage variation of the eigenfrequencies for the complete body of the guitar, with different hole sizes and orientations, with respect to the eigenfrequencies of the body with the solid plate. 44

3.21 MAC matrices comparing the modal shapes of the body with the metamaterials with those of the solid one. On the left the matrix for the case of the longitudinal holes (p=1), on the right the one for the case of the radial holes (p=1). 45

3.22 3D model of the guitar body with the bridge. The red arrow shows the direction of the applied load. 46

3.23 Normal displacement on the surface of the soundboard under the static load for different sizes of the holes. The top row shows results for the longitudinal holes, while the bottom row shows results for the radial holes. 47

3.24 RMS value of the normal displacement on the surface of the soundboards, as a function of the effective density in the lower bout ρ_{eff}. The black dotted lines are constant-value curves of $\sqrt{1/(\rho_{eff}^3 w_{RMS})}$. The values they refer to are reported normalized by the value for the the solid top. 48

3.25 Values of $\sqrt{1/(\rho_{eff}^3 w_{RMS})}$ normalized to the value for the solid top (marked in the graph by a black asterisk). 49

3.26 Von Mises stress on the surface of the soundboard under the static load for different sizes of the holes. The top row shows results for the longitudinal holes, while the bottom row shows results for the radial holes. 49

3.27 Normal displacement on the surface of the soundboard for varying thickness of the central brace (brace 4), indicated as d. The soundboard used here is the one with longitudinal holes, $p = 1$. 50

3.28 Quadratic average over the lower bout of the difference between the displacements in the metamaterial soundboards and the solid plate, computed as in (3.2). The values are reported for varying thickness of the braces: these were altered in pairs, except for the central one. The solid lines represent the results of a best fit to a quadratic polynomial. A diagram of the 7 fan braces with the same color coding used in the plot is also shown. . . 51

3.29 Magnitude of the driving-point mobility at the bridge location, for the solid top and two of the metamaterial plates. Above the the first three peaks the shapes of the first three modes are reported. The first mode involves ”breathing” motion of the structure, with the top and back plate moving outwards in phase; The relative phase between the two plates is instead inverted in the second mode. 53

3.30 Magnitudes of the mobility at resonance for the first three peaks for the longitudinal holes, with varying hole size, reported as a function of the effective density. The asterisks correspond to the results for the body with the solid top. 54

3.31 Magnitudes of the mobility at resonance for the first three peaks for the radial holes, with varying hole size, reported as a function of the effective density. The asterisks correspond to the results for the body with the solid top. 54

3.32 Average of the mobility for varying hole size, reported as a function of the effective density. Results for both longitudinal and radial holes are reported. The horizontal dotted line represents the average of the mobility for the body with the solid top plate. 55

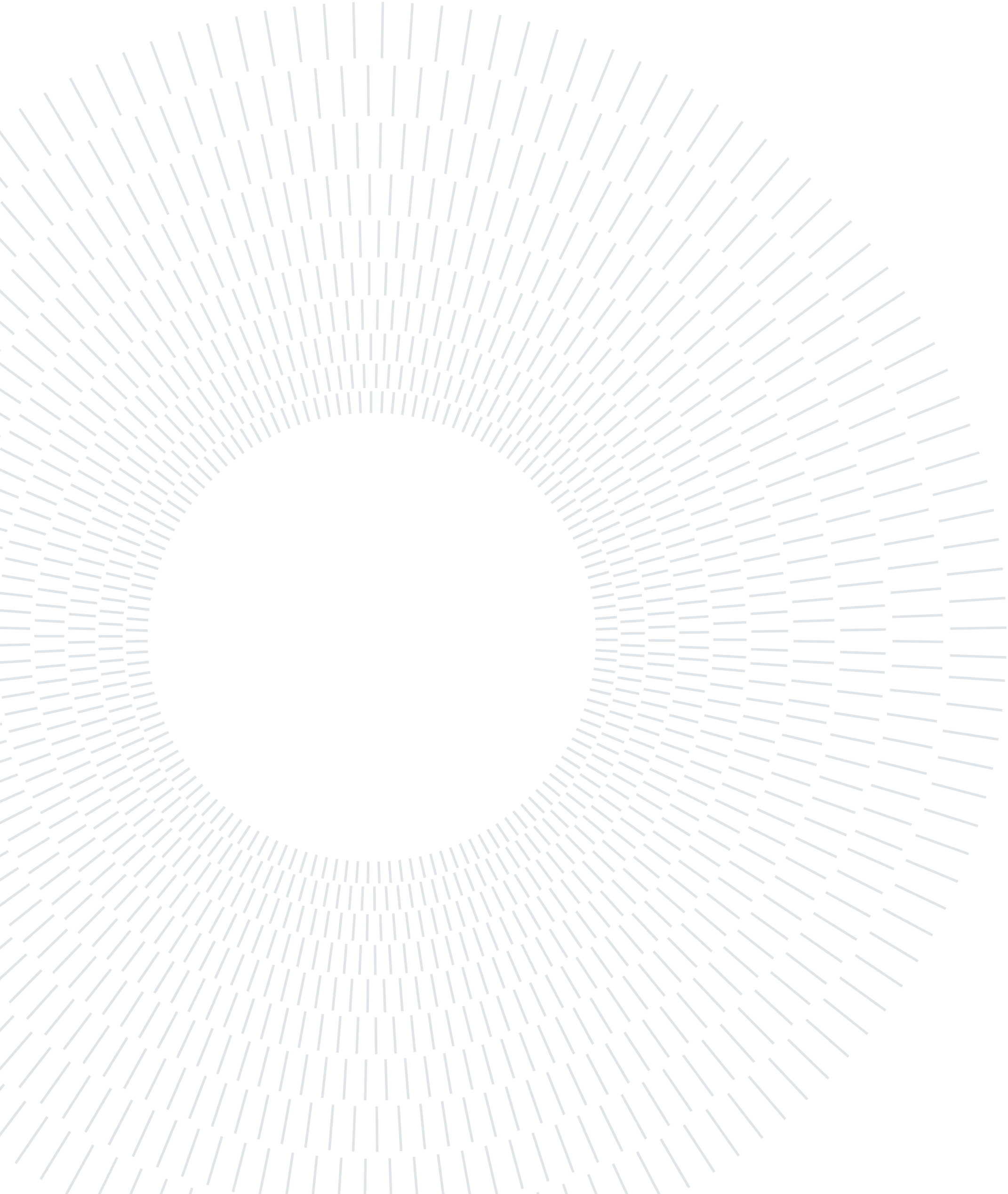

List of Tables

2.1 Properties of the materials chosen for the simulations. For each of the materials we define 9 constants, which, as explained in Chapter 1, are enough to completely characterize its elastic behaviour. 25

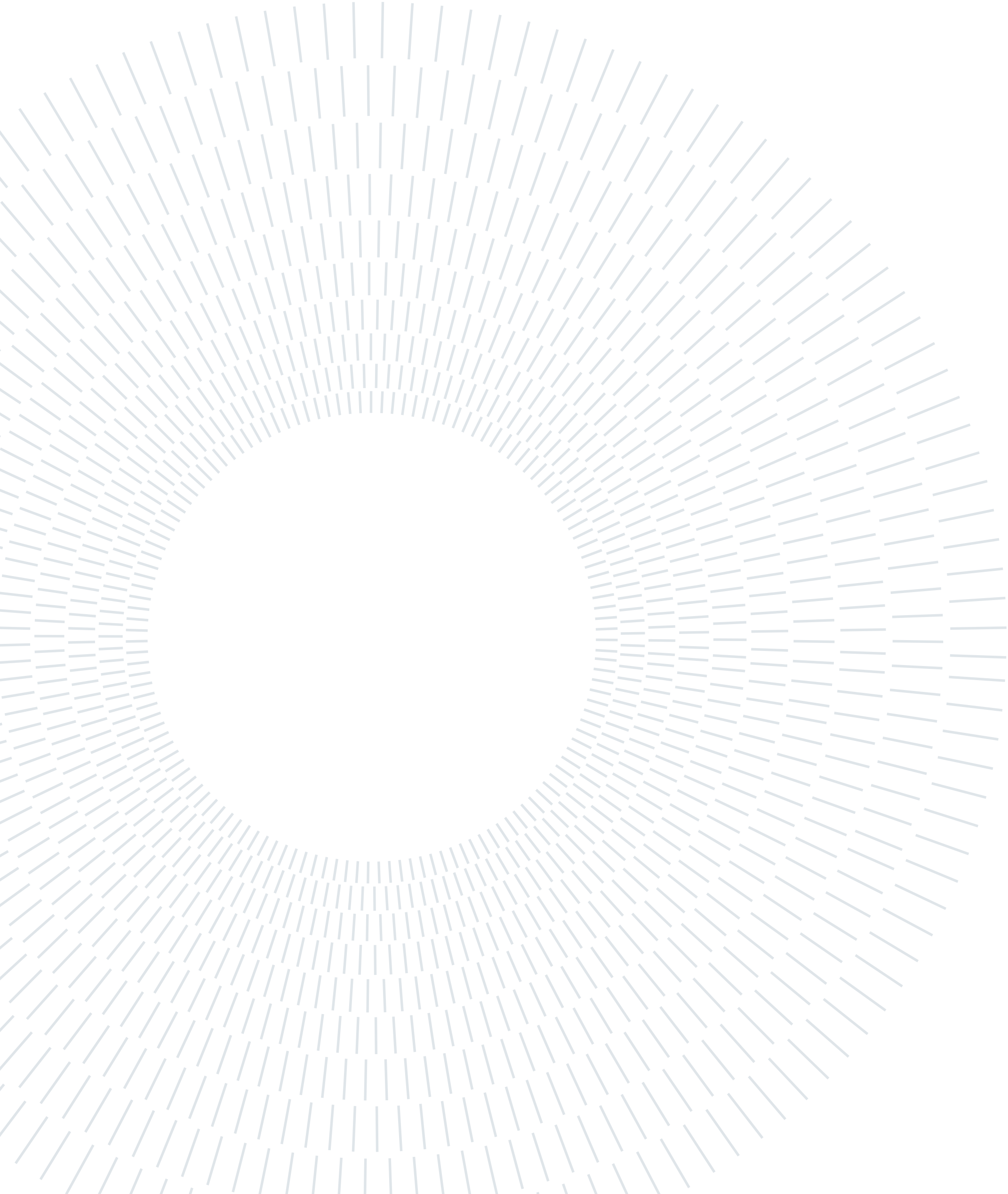

List of Symbols

Variable	**Description**	**SI unit**
σ_{ij}	stress tensor	Pa
ε_{ij}	strain tensor	-
A_{ijkl}	elasticity tensor	Pa
λ	Lamé's first parameter	Pa
μ	Lamé's second parameter	Pa
E	Young's modulus	Pa
ν	Poisson ratio	-
G	Shear modulus	Pa
w	Out-of-plane displacement	m
ρ Mass density	kg m^{-3}	
h Plate thickness	m	
D	Bending stiffness of a thin plate	Nm
$\boldsymbol{Y}$	Mechanical admittance/mobility	m s^{-1} N^{-1}
$\boldsymbol{v}$	Velocity	ms^{-1}
$\boldsymbol{F}$	Force	N
n	Modal density	s
R	Sound radiation coefficient	m^{4} s^{-1} kg^{-1}
a	Semi-major axis of the holes	m
b	Semi-minor axis of the holes	m
p	Scaling parameter	-
$\bar{w}$	Quadratic mean of w over the plate's surface	m
C	Damping matrix	kg s^{-1}
K	Stiffness matrix	kg s^{-2}
β	Stiffness-proportional damping coefficient	s

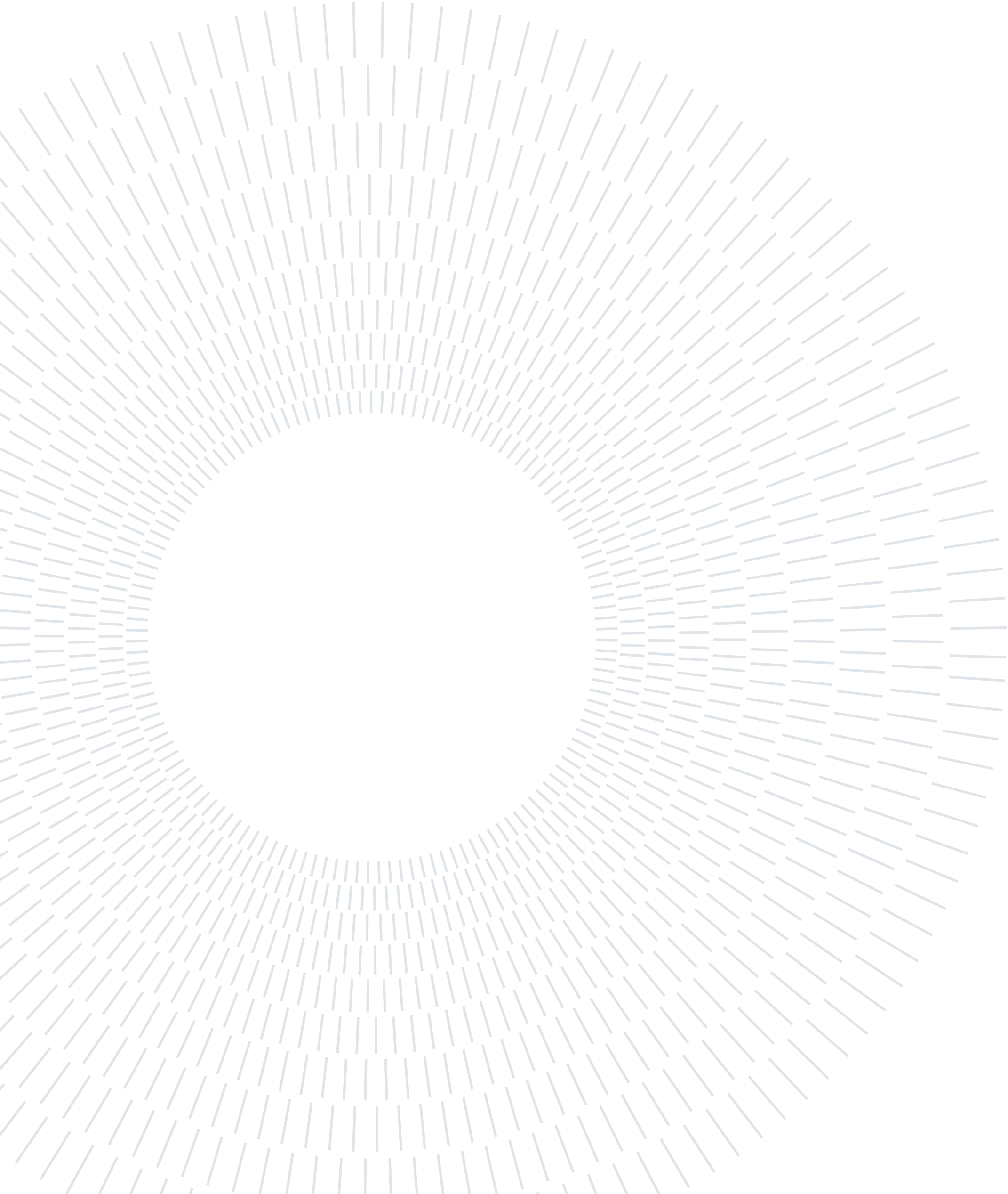

Acknowledgements

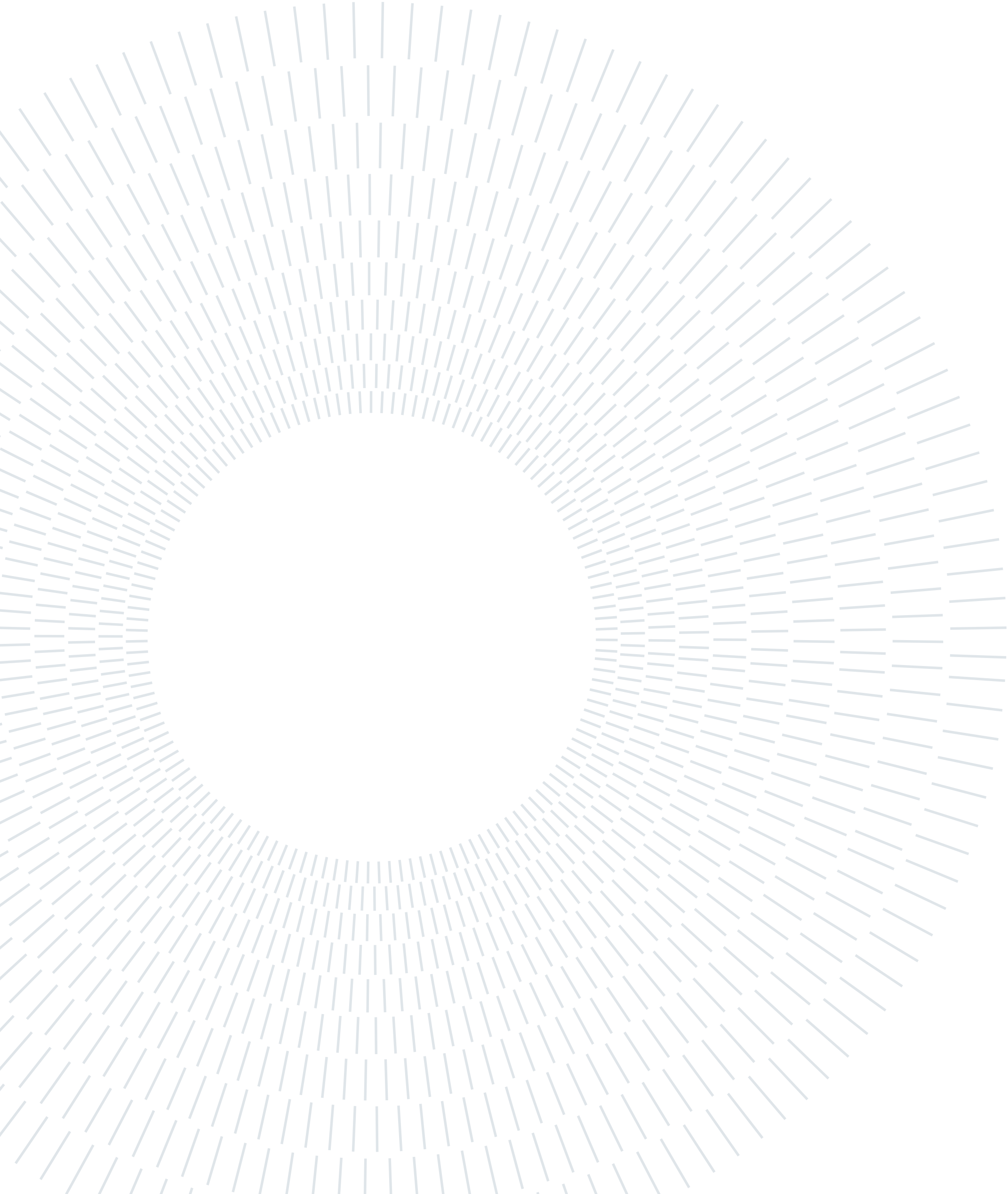Here you might want to acknowledge someone.